**The Thesis Committee for Anna Gabrielle Kladzyk**
**Certifies that this is the approved version of the following thesis:**

# Using high-resolution topography for advancing the understanding of mass and energy transfer across landscapes

**APPROVED BY**
**SUPERVISING COMMITTEE:**

**Supervisor:**

Paola Passalacqua

David Maidment

# Using high-resolution topography for advancing the understanding of mass and energy transfer across landscapes

**by**

**Anna Gabrielle Kladzyk, B.S.**

**Thesis**

Presented to the Faculty of the Graduate School of

The University of Texas at Austin

in Partial Fulfillment

of the Requirements

for the Degree of

**Master of Science in Engineering**

**The University of Texas at Austin**

**May 2015**

# Dedication

To Professor Liliana Marín

## Acknowledgements

I would like to express my deep gratitude to my advisor, Dr. Paola Passalacqua, for her guidance, support, and inspiring energy. Her mentorship has been a critical aspect of my success in the EWRE program and her thoughtful feedback offered an invaluable contribution to this research. Her dynamic instruction and example have expanded my skills in technical analysis and honed my communication abilities.

Thanks to several funding sources, including a generous grant from the National Science Foundation (GSS/BCS 1063228), and the Thrust 2000 James and Marie McNeil Endowed Graduate Fellowship in Engineering, this master's work has been made possible. Further support from the USGS Powell Center gave me the opportunity to travel to Ft. Collins, CO to spend a week in discussion and collaboration with various experts and exceptional scientists in the USGS Powell Center Working Group.

Many thanks to the entire Passalacqua research group for their excellent feedback during this research process. I would like to extend a special thanks to Harish Sangireddy for his willingness to discuss concepts, methods, and issues that came up during this research, as well as for mentoring me as I learned to use GeoNet. Sincere thanks to Dr. David Maidment for his insightful comments on this manuscript and numerous illuminating talks we had regarding my research and future work in the water resources engineering field.

Finally, thanks very much to my family and friends for their endless support over the past two years. Thanks to Bret for his encouragement, patience, and discerning counsel. Thanks to my dad, Frank, for always answering when I called during a bout of insecurity or frustration, and for his unwavering confidence in me. Thanks very much to my sister, René, for her brutally honest editing ("this sounds like a passage from

Napoleon Bonaparte's diary") and always excellent advice. Finally, thanks very much to the EWRE community: my inspiring student colleagues and the expert faculty—especially to Dr. Desmond Lawler for his exceptional commitment to my growth as an engineer and critical thinker.

# Abstract

## Using high-resolution topography for advancing the understanding of mass and energy transfer across landscapes

Anna Gabrielle Kladzyk, M.S.E.
The University of Texas at Austin, 2015

Supervisor: Paola Passalacqua

Channel networks are a critical means of mass and energy transfer across the landscape. High resolution topographic imagery derived from lidar scans, provides new opportunities in the observation and analysis of these processes, especially as the resolution of these data is proportionate to channel and hillslope process scales. Channel feature extraction algorithms supply a method with which to analyze hydrologic and geomorphic processes; automatic, open-source frameworks such as GeoNet aim to provide a reliable platform for this task to the academic, public service, and professional communities. In this thesis, the GeoNet algorithm is tested across different types of landscapes and data resolutions. Innovative analysis methods are also assessed within the framework in order to advance the method in parallel with advancing understanding of channel processes and improving technologies.

The goal of this research is to assess GeoNet performance across landscape type in terms of relief, vegetation, and anthropogenic influence and make recommendations for future development of the algorithm and the GeoNet user community. An alternate

spectral analysis-based filtering method is tested, as well as curvature-based filtering of erroneously identified channel heads. Results from alternate filtering testing indicate that the nonlinear Perona-Malik filter is superior to a spectral-based filtering approach. The use of a contour curvature threshold is not wholly successful at removing spuriously identified channel heads in natural landscapes. This research also introduces the analysis of urban landscapes into the GeoNet repertoire, and examines the effects of data resolution on feature extraction therein. An urban dataset from the Austin, TX area is tested and the optimal settings for GeoNet are identified; field work at the site is used to validate the results. The recommendations resulting from this work aim to improve in the functionality and versatility of GeoNet, and enhance accessibility for the user-community.

# Table of Contents

# List of Tables

# List of Figures

# Chapter 1: Introduction

Processes that facilitate mass and energy transfer involve complex climatic, hydrologic, and geologic interactions occurring over diverse space and time scales. Yet these complex processes are traceable; process signatures are embedded in the landscape as channel networks. Channel networks delineate dynamic pathways through which mass and energy transfer processes occur and evolve. For water resources management, observations of channel network structure and changes therein, provide critical insights into river basin morphology.

Feature extraction from high resolution imagery data allows us to identify critical channel network features [*Montgomery & Foufoula-Georgiou*, 1993]. Observable or measureable parameters from this data that define drainage basins include: terrain slope and curvature, drainage density, hillslope length, and vegetation [*Tarboton et al.*, 1991; *Dietrich et al.*, 1993; *Tarolli & Dalla Fontana*, 2009; *Passalacqua et al.*, 2014]. The identification of these features illuminates patterns of mass and energy transport across the terrain. Improved understanding of these transport processes provides critical insights into river basin morphology and informs water resources management. Applications for the automatic extraction of channel features from high resolution imagery are extensive, and include: design and implementation of infrastructure, restoring and protecting vulnerable ecosystems, and preparing for and mitigating extreme climate events [*Hudak et al.*, 2009; *Bates et al.*, 2010; *Jaboyedoff et al.*, 2010; *Hyde et al*., 2014].

## LIDAR DATA: SHIFTING PARADIGMS

The advent of high-resolution imagery data obtained from advanced scanning technologies engendered new capabilities with which to observe topographic features at a landform process-scale [*Roering et al.*, 2013]. Hydrologic and geomorphic land surface

forms and patterns can be identified and extracted from Light Detection and Ranging (lidar) imagery data via processing of the three-dimensional point cloud and analysis of the derived two-dimensional digital elevation models (DEMs). Vegetation and anthropogenic features are distinguished during the point cloud classification process, whereas channel networks and features, landslide scars, fault lines, and roads and ditches are identified using computational algorithms to analyze the two-dimensional DEM [*Lashermes et al.*, 2007; *Passalacqua et al*., 2010a; *Jaboyedoff et al.*, 2010]. The improved resolution of lidar (1-3 meter scale for airborne and cm/mm-scale for terrestrial or mobile lidar scans) is changing the means in which researchers and practitioners are capable of analyzing surface processes, however this emergent technology requires new tools and methodologies with which to use, store, and share this data.

Current limitations in the accuracy of features extracted from lidar-derived imagery are the result of several factors. The processing of the lidar point cloud includes the following steps: 'modeling of systematic errors', 'filtering', 'feature detection', and 'thinning' [*Meesuk et al.*, 2015]. Approximations are necessary to translate the raw point cloud into a computationally usable format, and subsequent filtering and pit filling performed on the DEM are required for efficient feature extraction. These operations may eliminate or distort important landscape features, and the balance between noise reduction and preservation of detail is a challenging aspect of this work, as the presence of noise influences the interpretation of local surface derivatives such as slope and curvature [*Lashermes et al.*, 2007]. Feature extraction algorithms are also limited in terms of scalability. Several algorithms have been tested at small scales (less than 5 $km^2$), but large scale applications are often limited computationally. Recent advances such as Python-based GeoNet, which relies on the open-source GRASS GIS for flow routing, and the parallel processing implementation of TauDEM offer new opportunities for feature

extraction on large scale datasets [*Youn et al.*, 2014; *Sangireddy et al*., in review]. High-resolution imagery provides terrain data at a resolution appropriate for interpreting information about surface processes and hydrologic connectivity, but evaluation and further development of features extraction tools is necessary to advance robust analysis frameworks for diverse landscape types and scales.

## RESEARCH GOALS

This research addresses three tasks; the first objective being the assessment of a feature extraction algorithm (GeoNet) in diverse landscapes and at different resolutions. The automatic extraction of channel features from large data extents and at finer resolution has applications in many fields of water resource management and planning. DEMs of two different resolutions are tested in this study. Differences in terrain type also pose challenges for feature extraction algorithms. *Passalacqua et al.* (2012) showed that different curvature computation methods can be used to improve channel extraction results depending on whether the landscape is predominantly undeveloped or includes anthropogenic features. A motivation for the research presented in this thesis stems from feature extraction results in low relief regions with engineered features in which the roads and irrigation canals are incorporated into the final channel network. This research further examines feature extraction performance across landscape type, and the datasets used exhibit diverse characteristics in terms of relief, vegetation, and anthropogenic influence. The study sites examined here include complex mountainous, moderate relief, and urban landscapes.

The remaining goals of this work are related to the application of GeoNet for researchers and practitioners. The second objective is to create guidelines for different aspects of feature extraction tools for LIDAR practitioners. These workflows provide

guidance in terms of customization of parameters within the feature extraction framework given the terrain type. Finally, the third goal of this research is to recommend directions for the improvement of these tools in terms of scalability and user-friendliness.

## SIGNIFICANCE OF WORK

The significance of this research lies in the value of improving algorithms which automatically identify and support monitoring of channel features and other landscape forms. The ability to observe and study these features from high resolution imagery can facilitate improved understanding of river basin morphology. This research also has application in engineering and watershed science applications. Flood mitigation can be improved with the ability to observe and monitor channel network features. Tools which identify the most upstream point of the channel, or the channel head, have important implications for mitigating mass-wasting events. These events often initiate due to disturbances in the most upstream portion of the channel structure where concentrated flow and erosion begin, therefore tools which can extract the locations of channel heads over time and space can be a useful risk warning measure. In broader terms, feature extraction from high resolution imagery already plays a critical role in water resource management and planning. Improvements in the functionality and versatility of these frameworks will inform more integrated and holistic resource management and risk mitigation strategies.

# Chapter 2: Literature Review

As digital terrain data became more widely accessible in the late 20th century, the development of algorithms for extracting channel and drainage basin information from this data was recognized as an important tool for examining fluvial mass and energy transport in drainage basins. *Montgomery & Foufoula-Georgiou* (1993) reviewed several early methods for identifying channel heads and networks from DEMs, and defined two important model assumptions: (1) channels initiate when an erosional threshold has been crossed, which led to a slope-dependent definition of channel initiation in line with the *Horton* (1945) theory of basin evolution, and (2) channel initiation occurs when there is a shift in the dominant sediment transport process. The difference between these two methodologies is expressed in the critical support area that drains to the channel head location. For the first case (slope-dependent) the critical support area changes with gradient; in the second case the critical support area is constant [*Montgomery & Foufoula-Georgiou*, 1993].

*Tarboton et al.* (1991, 1992) developed a channel feature extraction algorithm (TauDEM) which assumed a constant critical support/drainage area for channelization. In this framework the model is run for an initial area, then again for several different area values. *Tarboton et al.* (1991) used a sum of the squares approach to fit a line to the averaged "link slopes" (defined as the average slope along the distance between two confluences), and then plotted this versus corresponding source areas from the model runs. The authors recommended the inflection point in this graph to be used as the critical source area. The limitation of this method, as defined by *Montgomery & Foufoula-Georgiou* (1993), concerned bias introduced by the initially assumed source area which propagated into subsequent values of link slopes calculated from the initial channel

network based on the assumed area. The necessity to define a source area for channelization is an ongoing challenge in the development of algorithms which automatically identify channel features, and field data for channel heads and their source areas within a dataset are an invaluable asset in this task.

A major contribution to the task of automatic feature extraction was the identification of likely channelized features based on curvature, developed by *Lashermes et al.* (2007). The wavelet analysis method addressed the influence of elevation noise on surface derivative computations (e.g. slope and curvature) by filtering the elevation data, and calculating slope and curvature. The authors proposed an analysis of the probability density function of curvature in which the quantile-quantile plot of local curvature versus the standard normal variate was plotted. From the plot, an inflection point was identified where curvature values deviated in the positive direction from the standard normal. This led to a curvature-based threshold for likely channelized pixels, which has been applied by several other authors.

Building on several studies [*Montgomery & Dietrich*, 1988; *Montgomery & Foufoula-Georgiou*; 1993, *Lashermes et al.*, 2007; *Giannoni et al.*, 2005], *Passalacqua et al*. (2010a) developed an automatic channel network and channel head extraction algorithm, GeoNet, using high-resolution DEMs derived from lidar data. In the first step of GeoNet, the DEM is filtered to reduce small-scale noise and artifacts from lidar pre-processing present in the landscape image. Next, a statistical analysis of curvature of the surface is conducted in accordance with the method proposed by *Lashermes et al.* (2007). *Passalacqua et al*. (2010a) used the quantile-quantile plot of local curvature versus the standard normal variate to identify positive deviations (convergent, likely channelized) as well as negative deviations (divergent, likely ridged). Convergent pixels identified in this process form the first estimate of the channel network skeleton in GeoNet.

Once likely convergent pixels were identified and accumulation area calculated, a geodesic energy minimization method was used to trace pathways of minimal cost from the outlet of the basin up to the upstream extent of the channel, or the channel head locations [*Passalacqua et al*., 2010a]. The method was found to be particularly successful at predicting channel networks and channel initiation locations in complex mountain landscapes [*Passalacqua et al.*, 2010b]. For flatter landscapes exhibiting engineered features, the curvature calculation computation method was altered [*Passalacqua et al.*, 2012]. Recent improvements to the GeoNet algorithm, including the addition of a precursory median filter, have further enhanced its performance in low relief landscapes with anthropogenic features present [*Sangireddy et al.*, in review]. Details regarding curvature computation methods and filtering procedures available within the GeoNet algorithm are discussed in Chapter 3 of this study.

Recent studies have sought to improve and extend the use of surface curvature for channel feature extraction. *Sofia et al.* (2011) built on the statistical analysis of curvature for channel feature extraction developed in *Lashermes et al.* (2007) and *Passalacqua et al.* (2010a,b) used this in combination with an openness parameter, which measures dome-shapes (positive openness) or enclosures (negative openness) in terms of angles between the surface relief and horizontal distance, to identify convergence features in landscape. The purpose of the openness parameter addition was to create a method uninfluenced by artifacts or noise in the imagery data, and the authors found this to be successful in landscapes with minimal morphological complexity [*Sofia et al.*, 2011]. However, their results indicated that for more complex landscapes image filtering would still be necessary.

The scale dependence of curvature computation is discussed in *Sofia et al.* (2011), and is the focus of *Tarolli et al.* (2012). The latter authors sought to determine the

optimal scale for curvature calculation in order to identify land surface related to shallow landslide processes. After testing various sized kernel windows, *Tarolli et al.* (2012) found the optimum size window corresponds to 2-3 times the maximum size of the features of interest, and stated this size achieves a balance between minimizing noise in the results and over-smoothing. However, consistent with the findings of *Sofia et al.* (2011), the authors recommend filtering procedures for more complex morphologies. The filtering procedures used to address this issue in GeoNet are discussed in Chapter 3 of this report.

An alternative to a curvature-based channel feature extraction is spectral analysis. This framework has become a more widely-used tool to identify landscape features based on the theory that characteristic scales of these features can be identified in power spectra. *Booth et al.* (2009) employed spectral analysis to identify geomorphic features, specifically landslide scars, from high resolution imagery. The Fourier transform was used to translate the elevation data into spatial frequencies and then the characteristic scales of landslide features were identified in the power spectrum. *Perron et al.* (2008) used a two-dimensional Fourier analysis to examine the question of organizational patterns and spacing in land features. The authors identified wavelengths corresponding to ridge and valley features in this study as well. Spectral analysis is also widely used in filtering applications, and was recently applied in the analysis and reduction of noise in synthetic elevation data by *Pelletier* (2013). Spectral analysis of real elevation data, specifically the use of the optimal Wiener filter to do so, is the subject of Chapter 5 in this study.

Flat landscapes in agricultural and urban areas also pose unique challenges for feature extraction algorithms as discontinuities in drainage networks such as roads, ditches, and other structures, can both disrupt and/or be extracted as part of the drainage

network. As mentioned earlier *Passalacqua et al.* (2012) addressed this issue through the use of an alternate curvature computation method (Laplacian), which distinguishes between natural and artificial convergent features. *Cazorzi et al.* (2013) sought to identify flow paths in low-relief, agricultural regions where natural channel networks are augmented by engineered features. Along with detecting the drainage network, these authors identified network storage capacity based on the network length width and channel cross sections. Instead of using spectral analysis and a low pass filter, the authors addressed the presence of disruptive anthropogenic features by creating a "relative elevation attribute" map which is the difference between averaged elevation values within a certain radius and the DEM values. This normalization minimized the presence of larger-scale features.

The continued improvement of channel feature extraction algorithms has drawn on contributions from a broad array of fields and expertise. Classical methods employing curvature-based and drainage area thresholds are still in wide use, and refinements of these tools have expanded the applicability thereof. Advancements based on statistical methods, innovative parameterization, and spatial frequency analysis have also shown promise for the enhancement of these tools in parallel with the growth of high resolution imagery data processing and improved resolution. The remainder of this thesis is focused on assessing two recently proposed methods for improved channel feature extraction, and alternative approaches for extracting flow paths from urban landscape imagery.

# Chapter 3: Background

## Overview of GeoNet Feature Extraction Methodology

The GeoNet framework is an automatic channel feature extraction tool for high resolution imagery data, and is typically used on lidar-derived DEMs of meter scale resolution. For a full description of the theoretical background and algorithm details see *Passalacqua et al.* (2010a, 2010b). GeoNet can be summarized by the three major steps in the framework. The first of these steps is a filtering procedure to remove small-scale variability and/or noise in the DEM image. The two filtering methods available in GeoNet are a linear Gaussian filter and a nonlinear Perona-Malik filter. The Gaussian kernel equation used for filtering is:

$$h(x, y, t) = h_0(x, y) * G(x, y; t) \tag{3.1}$$

in which the original elevation $h_0(x, y)$ is convolved with the Gaussian kernel $G(x, y; t)$ of standard deviation $t$ centered at $(x, y)$ *Passalacqua et al.* (2010a). The expression for the Gaussian kernel is expressed as:

$$G_{x,y,t}(u, v) = \frac{1}{2\pi t} exp\left[-\frac{(u - x)^2 + (v - y)^2}{2t}\right] \tag{3.2}$$

The Perona-Malik filter includes an edge-stopping function based on a percentile of slope values (typically set to the 90th percentile) which preserves important edge features (in a channel feature extraction context) such as channel banks and ridges. The filter equation is:

$$\partial_t h(x, y, t) = \nabla \cdot [p(|\nabla h|)\nabla h] \tag{3.3}$$

where the edge-stopping function is expressed as:

$$p(|\nabla h|) = \frac{1}{1 + (|\nabla h|/\lambda)^2} \tag{3.4}$$

The edge-stopping function references the constant, $\lambda$, which is typically set to the 90$^{th}$ percentile slope values.

Small errors or artifacts in the DEM resulting from the data collection or lidar processing can introduce erroneous results, particularly within the local slope and curvature computations. The following image depicts two examples of small scale noise that are advantageously removed with filtering.

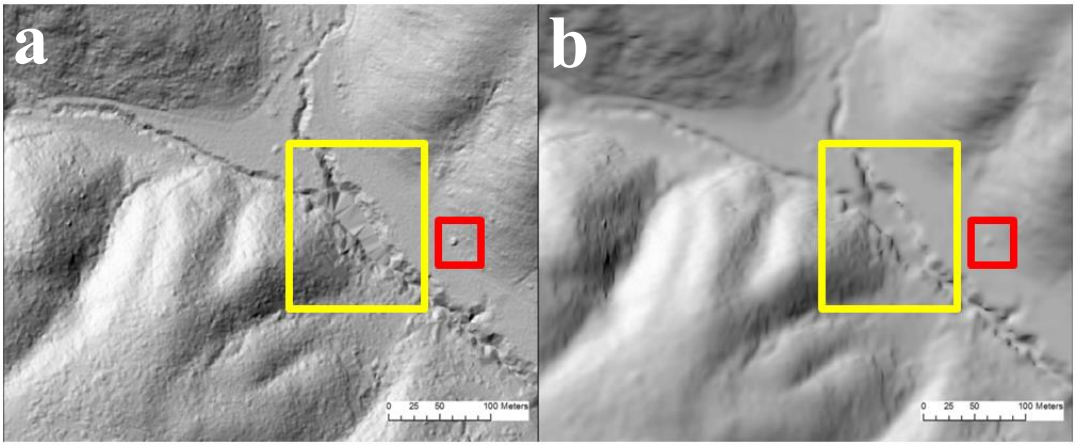


Figure 1: Image *a* shows an unfiltered hillshade for a portion of the Tennessee Valley DEM. In the yellow box there are noticeable sharp edges within the channel bed. In the red box in the left image there is a small artifact that may be the result of some misclassified vegetation in the point cloud data. The right image b shows the Perona-Malik filtered hillshade in which both of these features are smoothed along with other fine scale noise across the hillslopes and channel valley.

The second major step in the GeoNet algorithm is the identification of likely channelized pixels through a statistical analysis of curvature. There are two curvature computation methods currently available in GeoNet: Laplacian and geometric. Laplacian curvature $\gamma$ is the second derivative of the elevation $h$, and is expressed simply as:

$$\gamma = \nabla^2 h \tag{3.5}$$

whereas geometric curvature, $\kappa$, is normalized by the slope $|\nabla h|$ as shown in the following expression,

$$\kappa = \nabla \cdot \left( {}^{\nabla h}/_{|\nabla h|} \right) \tag{3.6}$$

The geometric curvature method has been shown to more accurately identify channel convergence in high relief, mountainous landscapes, whereas the Laplacian is more adept at identifying channel features in low relief landscapes where engineered features are present [*Passalacqua et al.*, 2012]. Likely channelized pixels are identified from a quantile-quantile plot of the curvature values versus the standard normal variate as discussed in Chapter 2. The pixels which deviate from the standard normal distribution in the positive direction (convergent) form the first estimate of the channel skeleton in the dataset.

The final major step in GeoNet is the extraction of the channel network and end point locations based on a global geodesic analysis of the landscape. First, flow routing is performed to calculate flow accumulation area for the entire dataset; the D-infinity algorithm is used in the MatLab-based GeoNet version, and a multiple flow direction algorithm is used in Python-based GeoNet (via GRASS). The geodesics then define the

energy cost for water to travel along any given path in terms of curvature and flow accumulation area. The cost function for the geodesics is defined as follows:

$$\psi = \frac{1}{(\alpha \cdot A + \delta \cdot \kappa)} \tag{3.7}$$

where $A$ is flow accumulation area $\kappa$ is curvature and $\delta$ and $\alpha$ are constants to correct for differing units in the curvature and accumulation area. Water will take the most efficient path from an upstream area to an outlet; therefore the paths of least cost will follow pixels with high curvature values and high flow accumulation values. Finally, a fast marching algorithm is used to finalize the channel network, and a search box scans the network for channel end points. Raster files (.tif) are written out and saved of various outputs from the algorithm, including slope, flow accumulation area, curvature, geodesic distance, and the channel skeleton. Vector files (.shp) are also written out of the channel network and end point locations.

# Chapter 4: Contour Curvature

## 1. OBJECTIVE

***Determine whether contour curvature can be used to filter out spurious channel heads in algorithm results***

## 2. METHODS

Contour or tangential curvature has been used in other channel extraction algorithms to filter erroneous channel head results [*Pelletier*, 2013; *Clubb et al.*, 2014]. Contour curvature is defined as the second derivative of a normal plane tangent to the contour line of a surface [*Mitasova & Hofferka*, 1993]. High contour curvature values can be visualized on the land surface as locations where the contour lines form deep crenulations with sharp v-shapes. In the studies conducted by *Pelletier* (2013) and *Clubb et al.* (2014), contour curvature is used to eliminate spurious channel end points by designating a threshold of contour curvature and discarding end points with curvature values of less than the threshold. Both studies use a threshold value of 0.1. The use of contour curvature in a channel head filtering application is distinct from the curvature computation used to provide a first estimate of channelized pixels in GeoNet (geometric and Laplacian), as described earlier in Chapter 3.

Contour curvature was computed in the parallel to the method used by *Pelletier* (2013) and *Clubb et al.* (2014), and originally defined by *Mitasova & Hofferka* (1993) as:

$$K_t = \frac{h_{xx}h_y^2 - 2h_{xy}h_xh_y + h_{yy}h_x^2}{(h_x^2 + h_y^2)\sqrt{1 + h_x^2 + h_y^2}} \tag{4.2.1}$$

where $h$ is the elevation and the subscripts indicate first $(x, y)$ and second derivatives $(xx, yy, xy)$ in the specified direction.

The contour curvature equation was discretized and implemented into GeoNet and the values corresponding to the end point locations were saved as outputs. The end points with contour curvature values of greater than the threshold of 0.1 were distinguished from the other end points, and all points were plotted with contour lines at 10 meter intervals to confirm whether end points above the threshold were indeed aligned with deep crenulations in the contours. The discretized contour curvature algorithm was also checked with hand calculations of a small subset of the data to confirm accuracy in the discretized equation.

The datasets (described in section 3 of this chapter) used to examine contour curvature were also used in *Clubb et al.* (2014), which provided a means of comparison for the results. The user-defined flow accumulation area thresholds for each dataset were set to the minimum threshold area values corresponding to channel heads mapped in the field by *Clubb et al.* (2014).

## 3. STUDY SITES

Data for each study site used in this analysis were one meter resolution DEMs derived from airborne lidar scans. The contour curvature analysis focused on basins which exhibit complex, high-relief landscapes in Northern California, and basins amidst rolling low grade hills in the Midwest and Eastern U.S. The data are described below and grouped into the following two categories:

**(i) High relief (>250 m) and vegetative:** The Bald Creek and Cascade Ridge sites are highly forested with steep slopes, and lie within the Feather River basin in the Californian Sierra Nevada Mountains.

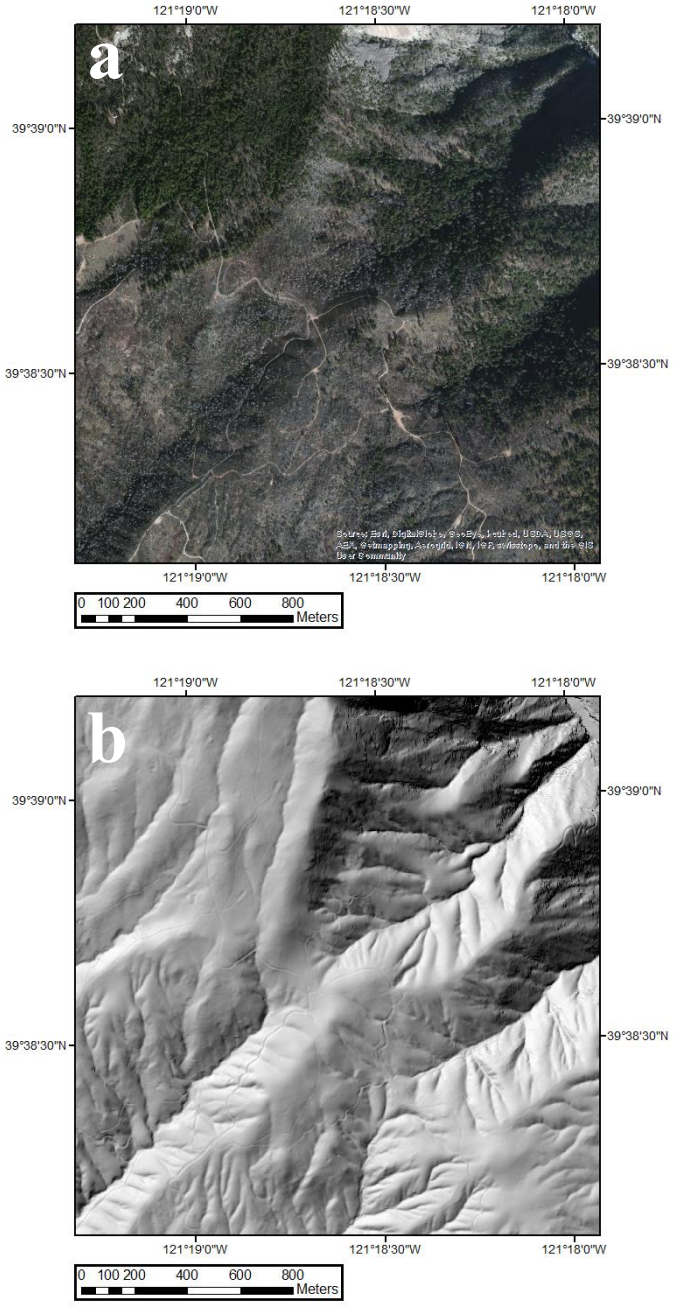


Figure 2: Image *a* shows satellite imagery of the Bald Creek site; *b* is the hillshade of the same extent.

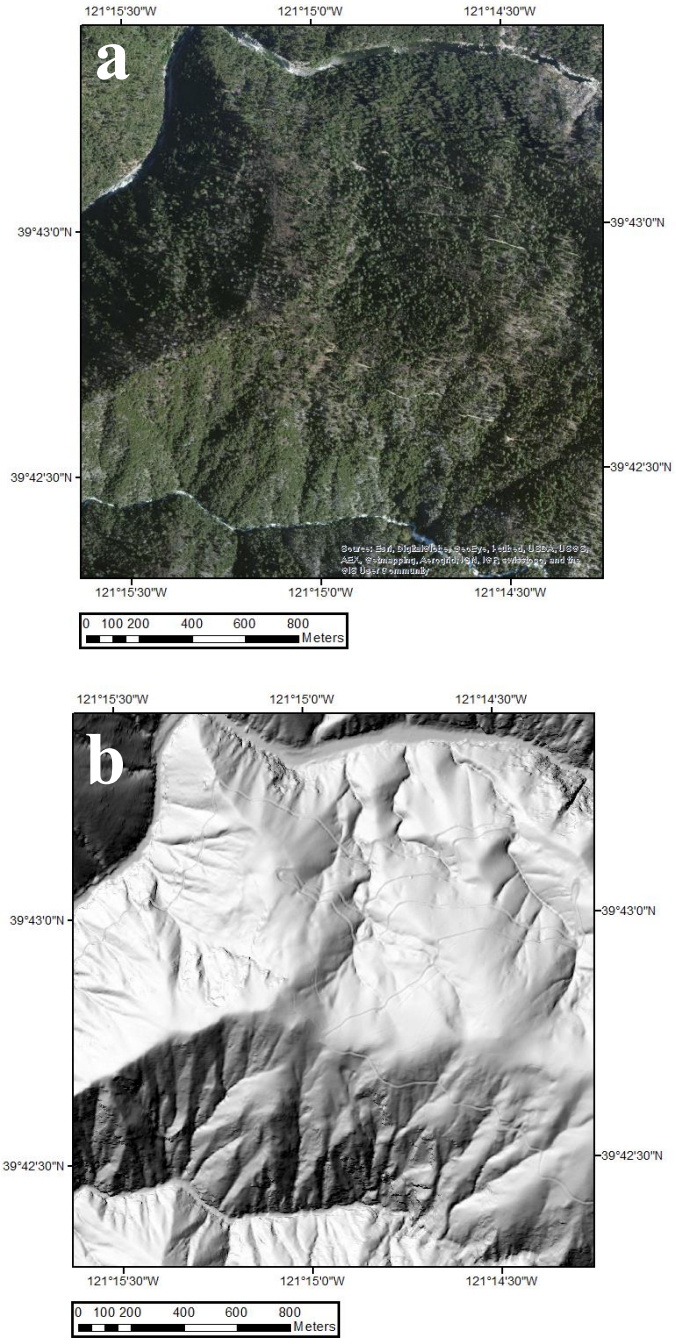


Figure 3: Image *a* shows satellite imagery of the Cascade Ridge site; *b* is the hillshade of the same extent.

The second category of landscape analyzed in the contour curvature portion is:

**(ii) Moderate relief (>50 m but <250 m) and vegetative with some engineered features:** The Piedmont, Virginia landscape is characterized as moderate relief with gently sloping plains and dense vegetation [*Clubb et al.,* 2014].

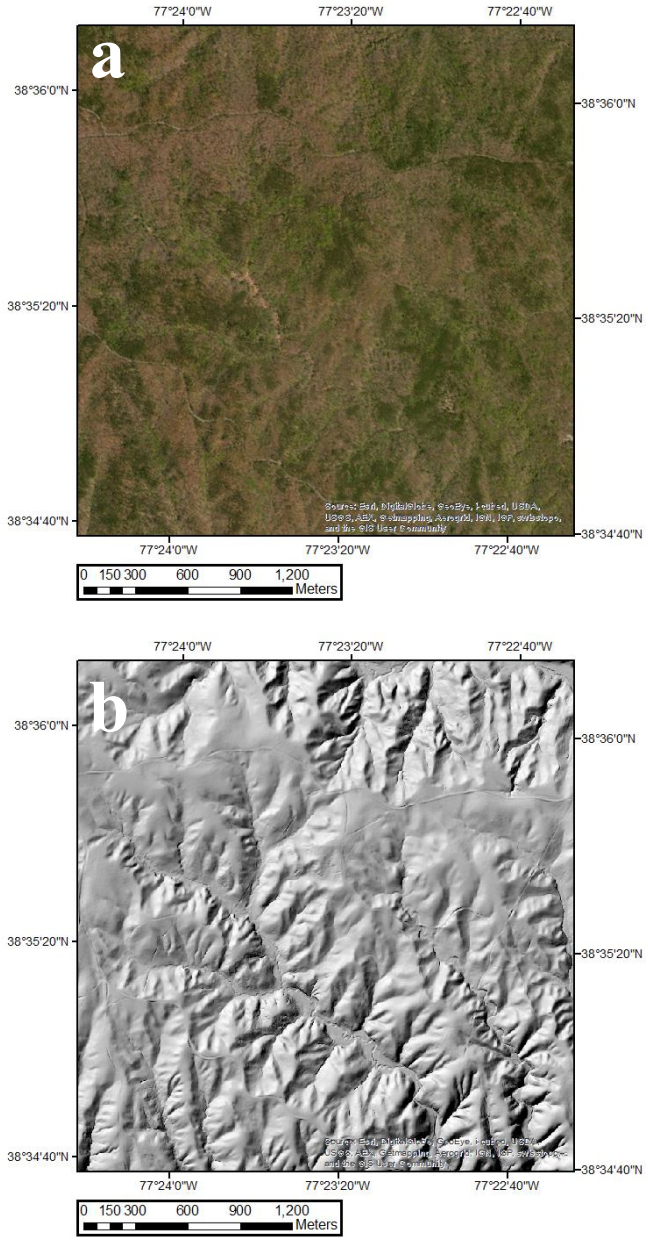


Figure 4: Image *a* shows satellite imagery of the Piedmont site; *b* is the hillshade of the same extent.

The Indian Creek site is located in the Wayne National Forest, Ohio and is a complex landscape with dense forest vegetation and moderate to steep slopes [*Clubb et al.,* 2014]. This landscape also presents roads and walking trails through the forest.

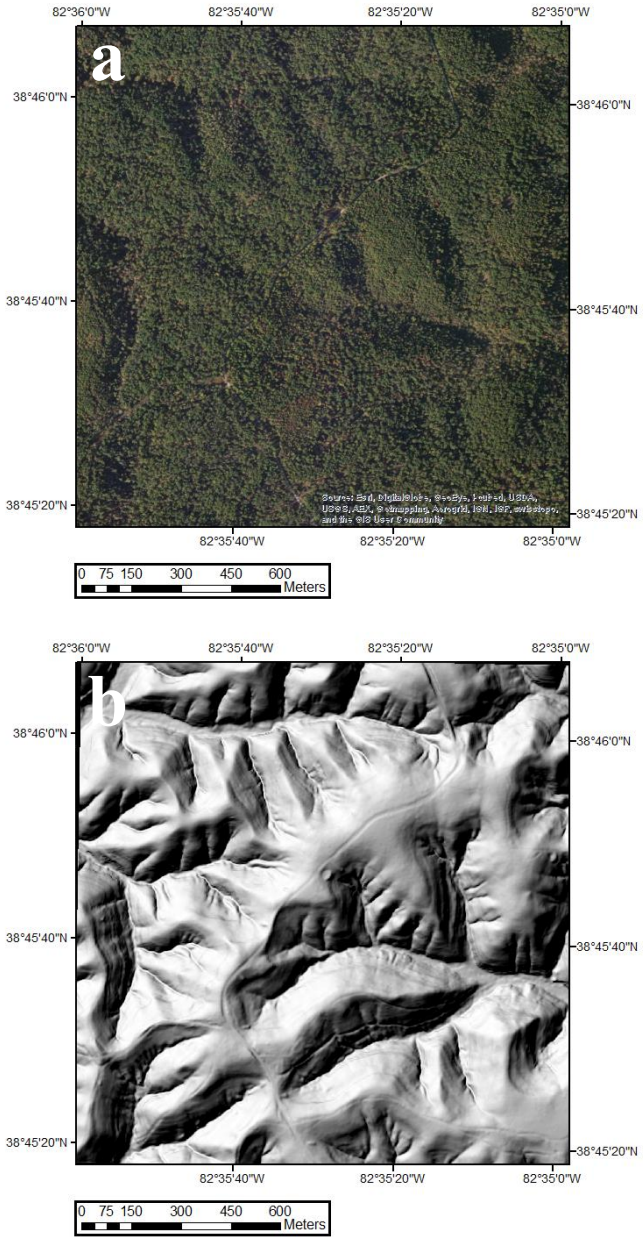


Figure 5: Image *a* shows satellite imagery of the Indian Creek site; *b* is the hillshade of the same extent.

Field surveyed channel head locations for Bald Creek, Cascade Ridge, Indian Creek were collected by *Clubb et al.*, (2014) and made available at (http://datashare.is.ed.ac.uk/handle/10283/524). Channel head locations for the Piedmont site were collected by *Julian et al.* (2012) and assimilated by *Clubb et al.* (2014) and are available at the same site. These field channel heads are used for a means of comparison in this study.

## 4. RESULTS

The channel end point results are shown for the basins with blue distinguishing contour curvature values of less than the recommended threshold of 0.1, and red identifying channel end points with contour curvature of greater than 0.1. The results for the complete datasets are shown here, along with more detailed views of each dataset.

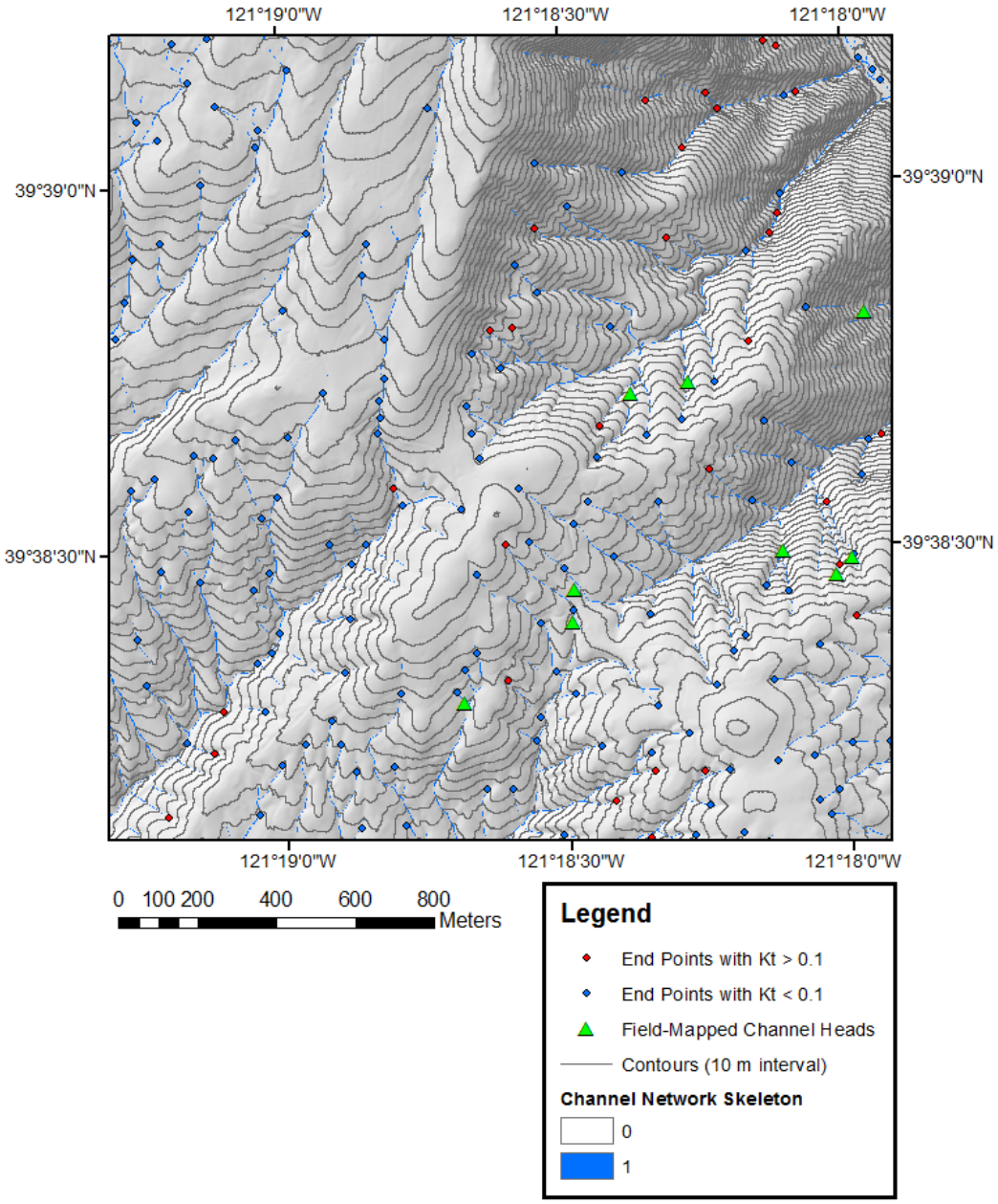


Figure 6: Map showing end point results for entire Bald Creek dataset. End points with contour curvature values of greater than 0.1 are shown in red, whereas those with contour curvature values of less than the threshold (and are hypothesized to be spurious) are shown in blue. Field-surveyed channel heads are also depicted in green.

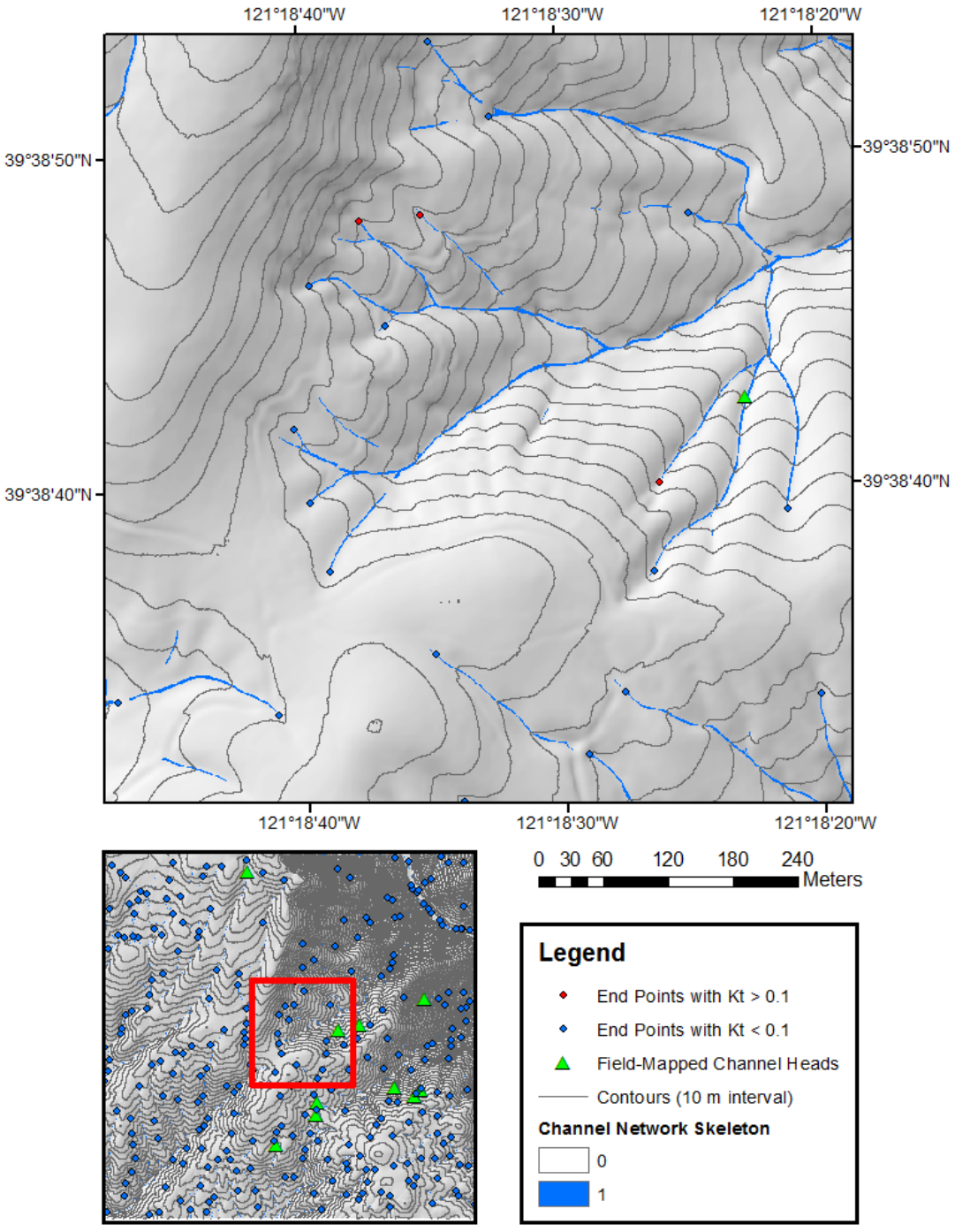


Figure 7: Map showing subset of results for Bald Creek dataset.

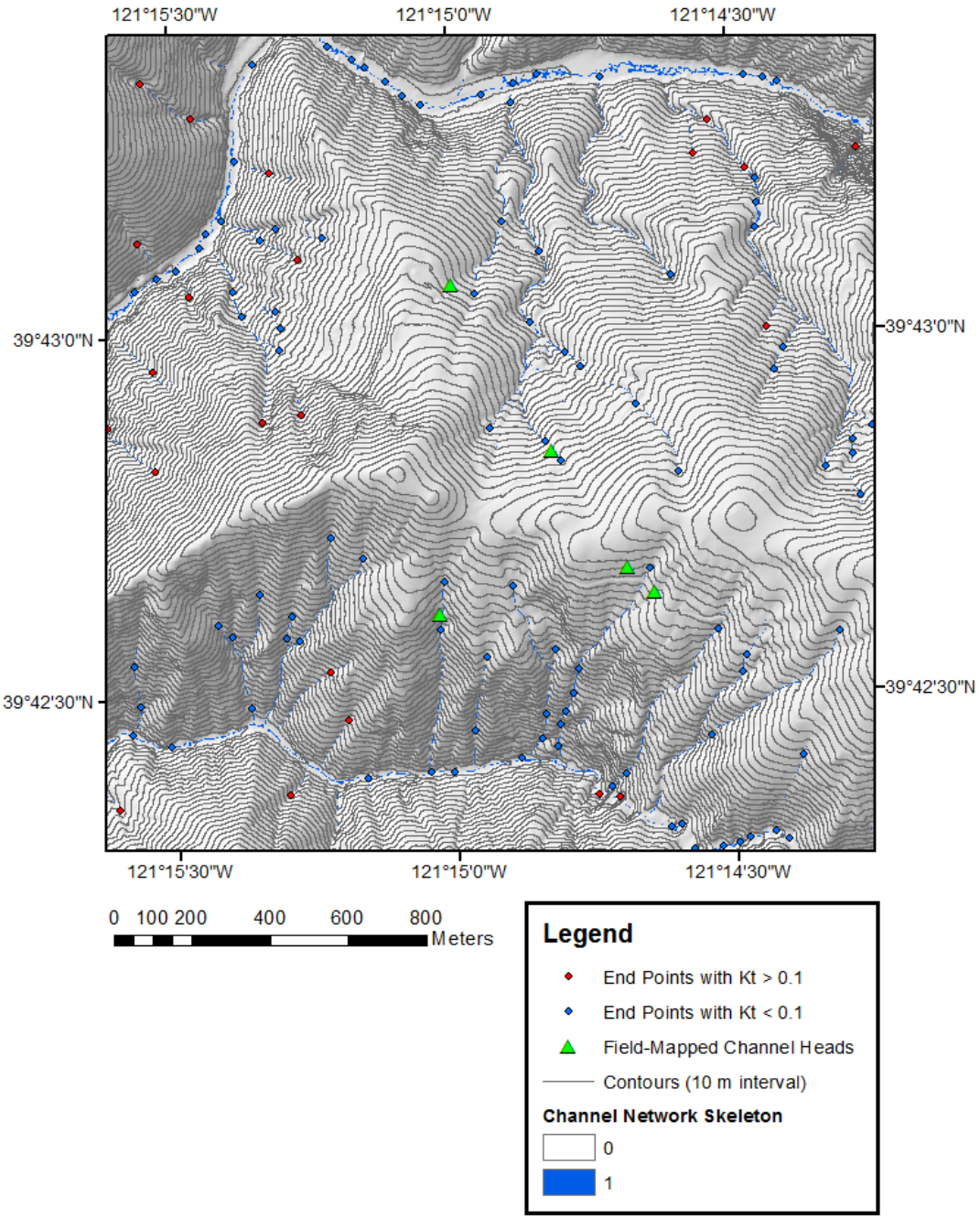


Figure 8: Map showing end point results for entire Cascade Ridge dataset.

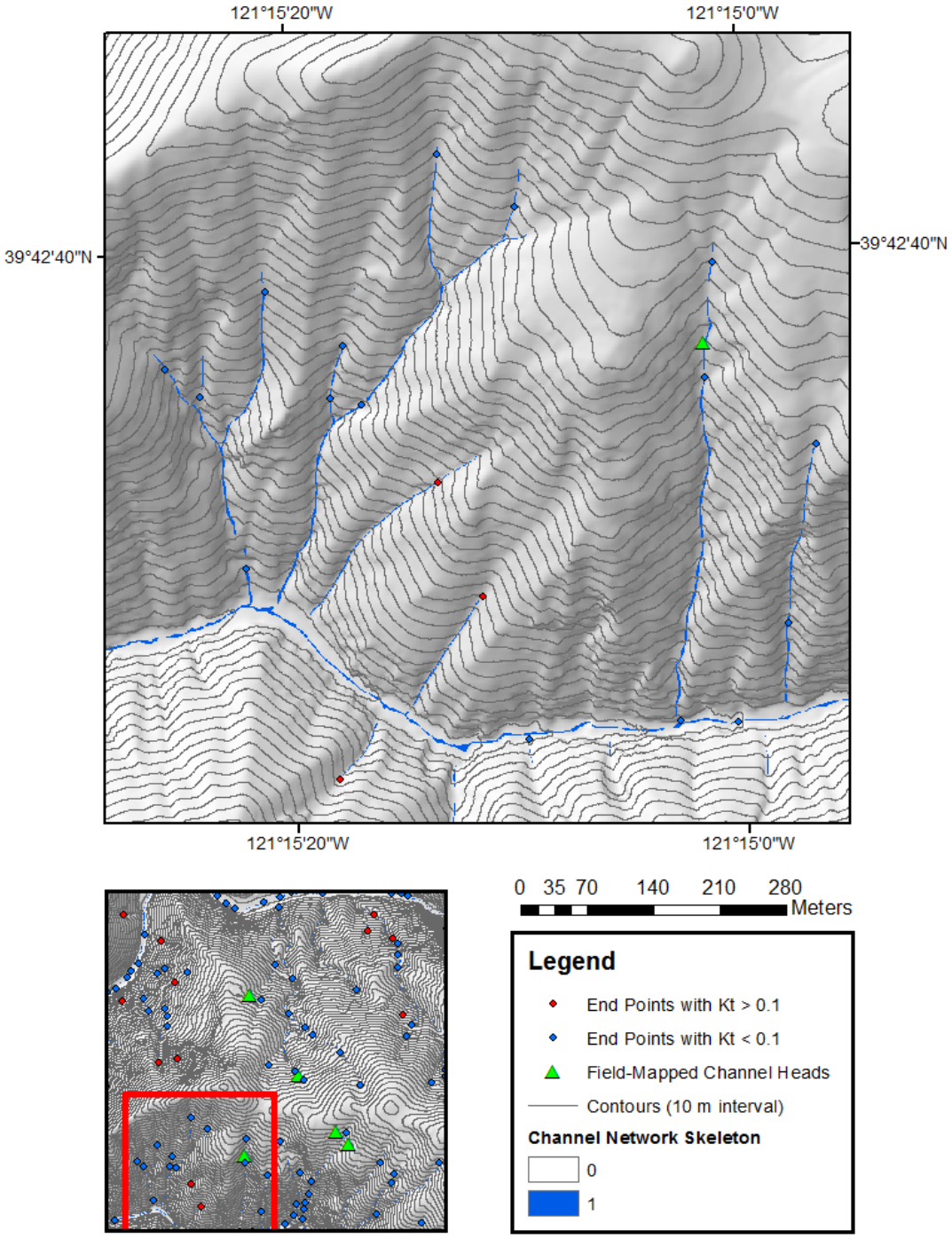


Figure 9: Map showing subset of results for Cascade Ridge dataset.

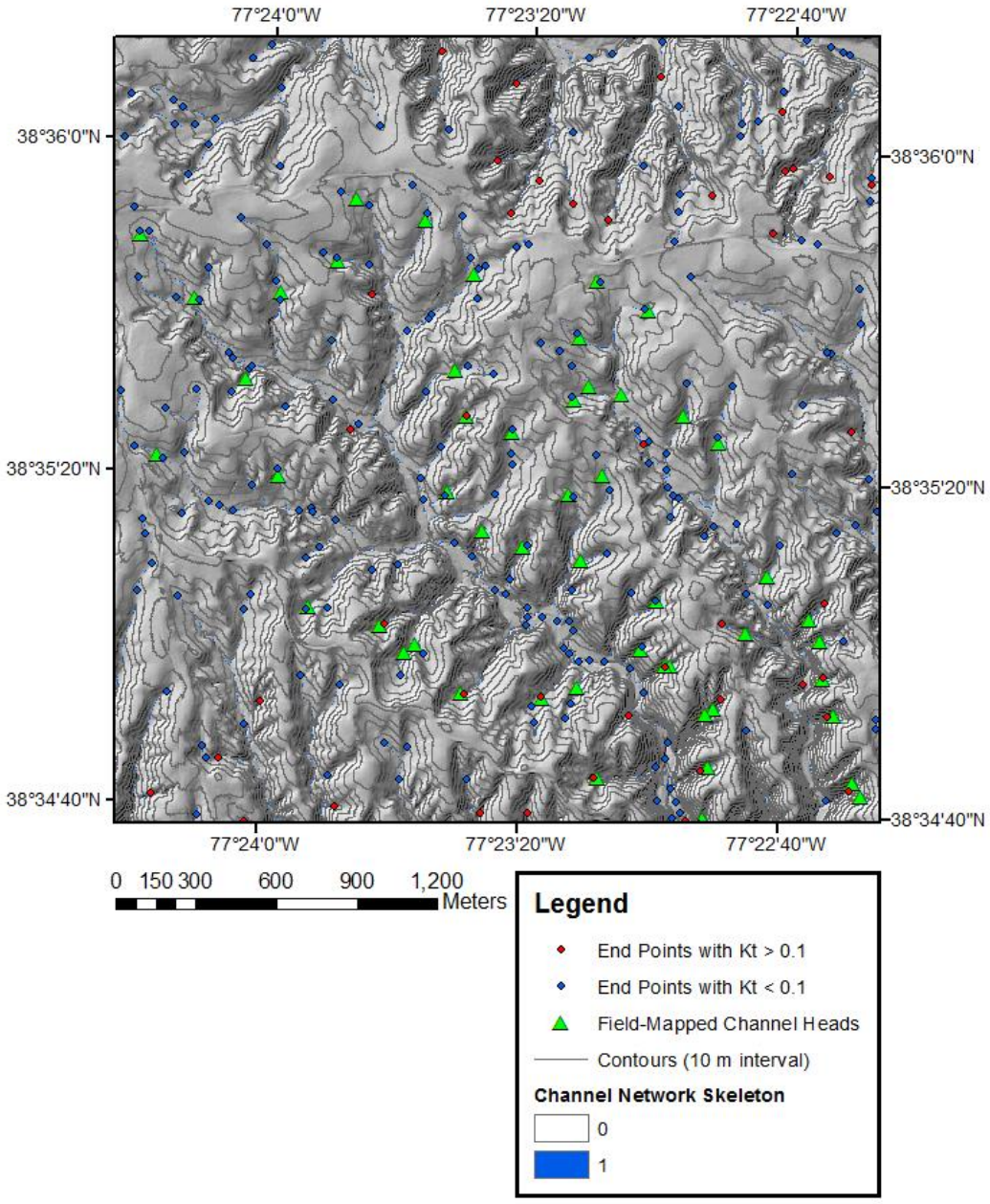


Figure 10: Map showing end point results for entire Piedmont dataset.

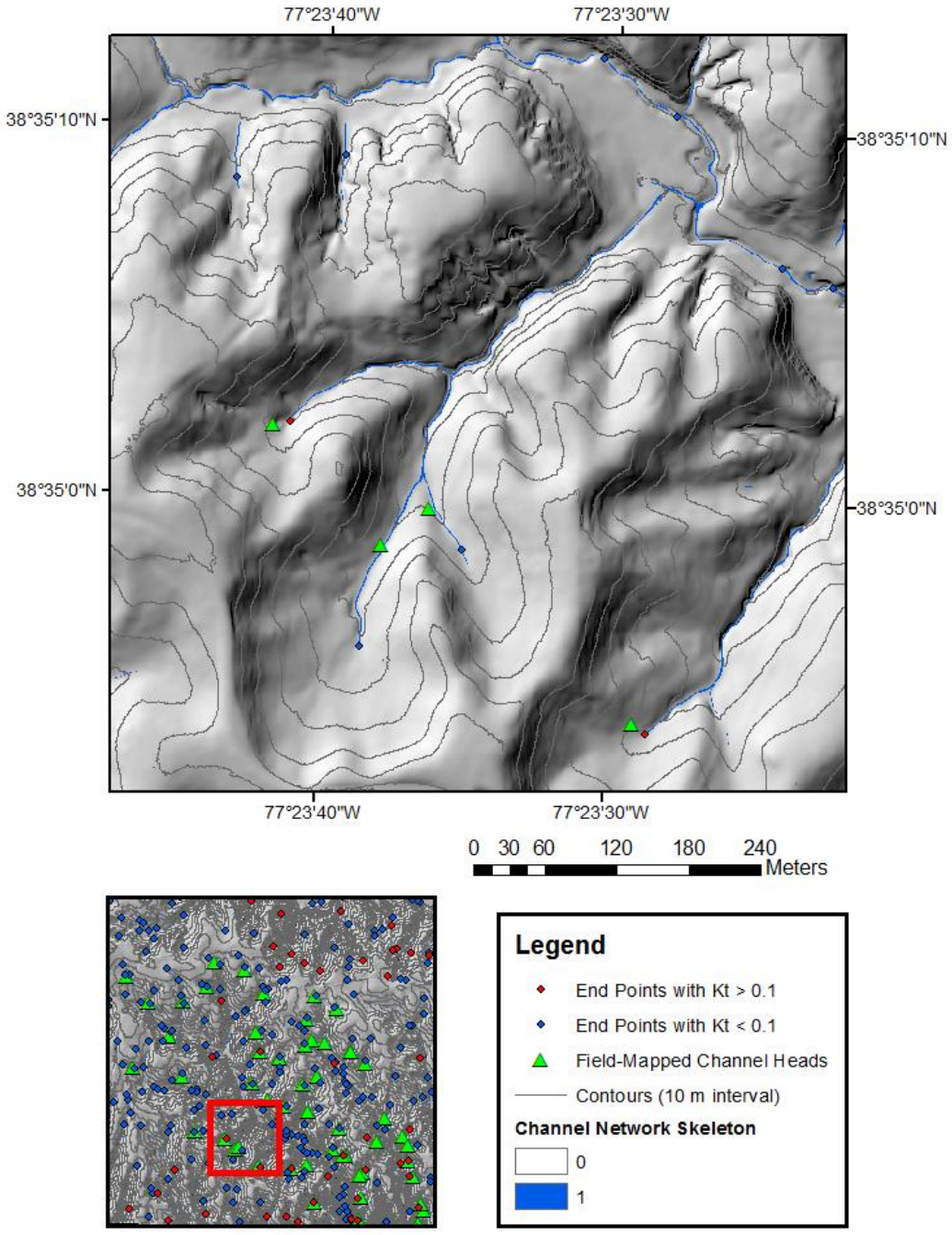


Figure 11: Map showing subset of results for Piedmont dataset.

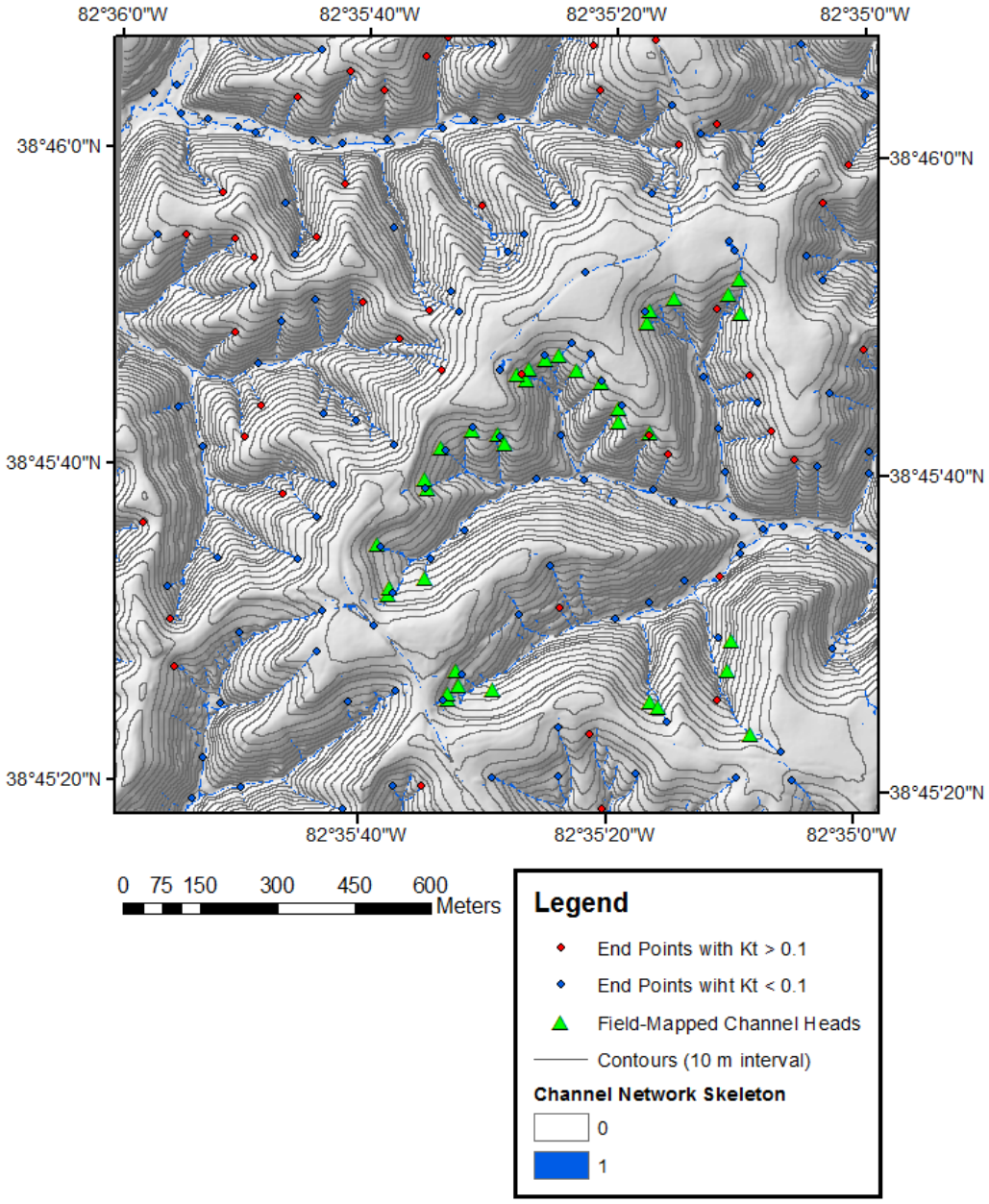


Figure 12: Map showing end point results for entire Indian Creek dataset.

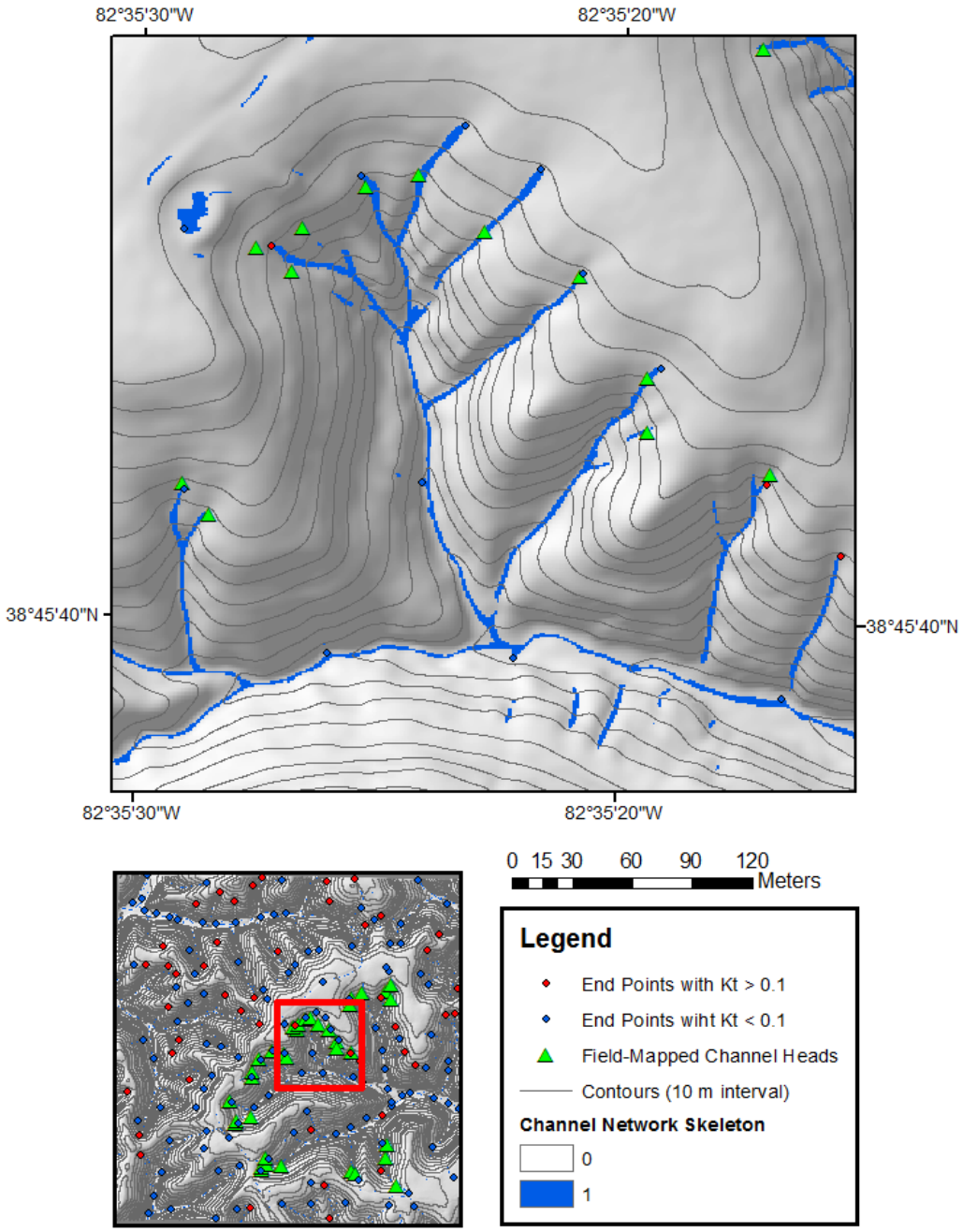


Figure 13: Map showing subset of results for Indian Creek dataset.

## 5. DISCUSSION

The results for contour curvature are evaluated based on comparisons between estimated channel end point locations with contour curvature values of greater than 0.1 and those with less than 0.1. The objective of setting this curvature threshold is to eliminate spurious channel head (end point) estimates as used by *Clubb et al.* (2014) and *Pelletier* (2013). The field-mapped channel heads assimilated by *Clubb et al.* (2014) are also used for comparison, though they are not consistently present throughout the entirety of each dataset. Recall that the minimum flow accumulation area threshold used for estimating the channel network is based on the minimum area value for the mapped channel heads, so when field heads are not present the most upstream pixel of the channel skeletons serves as the estimate for the channel head.

The detailed views of all the datasets (Figure 7, 9, 11, and 13) demonstrate end points with $K_t$ > 0.1 in agreement with the upstream-most channel pixels. However, several other channel end points with $K_t$ < 0.1 are also in agreement with channel end point locations. This is exemplified in the detailed view of the Piedmont dataset (Figure 11) for the two upstream areas in the southwest quadrant. These upstream regions of the channel network do not exhibit sharp crenulations in the contour lines. Views of the entire data extents (Figures 6, 8, 10, and 12) show end point locations with $K_t$ > 0.1 in the downstream valley portion of the channel, indicating that this method cannot be universally used to eliminate spurious channel head estimates, as pixels with high $K_t$ values may exist within the downstream channel sections.

These results show the contour curvature threshold does not successfully eliminate spurious channel heads in the natural landscapes examined here. Therefore, this method will not be implemented into the GeoNet framework. Pelletier (2013) used this procedure on synthetic landscapes where the upstream portions of valleys ended with a

sharp v-shape, and also employed an algorithm to trace the downstream channel beds and remove channel heads within, which may be why this method was more successful in that study.

# Chapter 5: The Optimal Wiener Filter

## 1. OBJECTIVE

***Assess the performance of the Optimal Wiener filter in GeoNet and determine if it has advantages in comparison with the Perona-Malik filter***

## 2. METHODS

### Filtering Process

The optimal Wiener filter (OWF) has been widely used in the fields of electrical engineering and image processing for over half a century. The filter identifies signal and noise scale in the power spectra and more gradually attenuates the noise frequencies in comparison with traditional band pass filters, resulting in a higher quality filtered image [*Wiener*, 1949]. More recently this filter has also been used in a spatial context to remove added noise in synthetic landscapes [*Pelletier*, 2013]. The OWF identifies elevation noise scales in the spatial frequency content of a landscape image and attenuates the frequencies of the small-scale variability (noise). *Pelletier* (2013) found this filtering scheme removed microtopographic noise as a component of a channel feature extraction algorithm for synthetic landscapes, and its efficacy in real landscapes is the subject of this chapter.

The following example of a synthetic landscape is used to illustrate the OWF methodology. Gaussian noise is added to a simple idealized ridge, and the original and noisy landscapes are shown in plan-view and as cross-sections of the ridge.

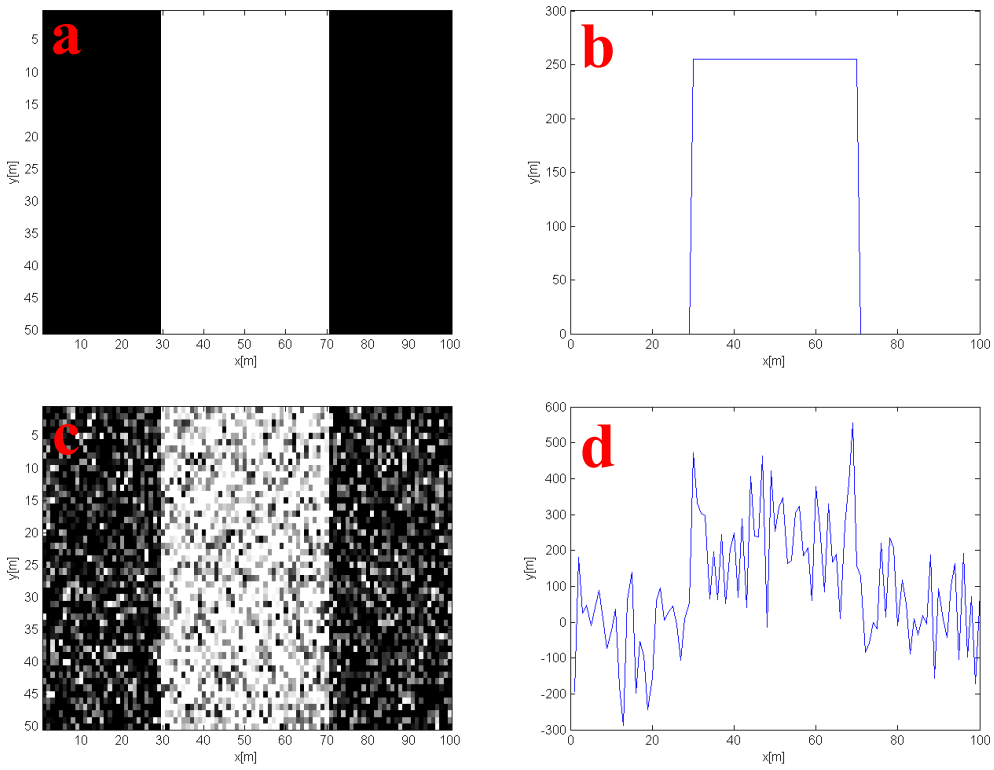


Figure 14: In *a* an idealized ridge is shown in plan-view, and the cross section in *b* shows the elevation beginning 0 m at the 0 m distance in the *x*-direction, and the ridge height begins at a uniform 250 m before decreasing abruptly again to 0 m. Iamges *c* and *d* depict the ridge in plan-view and as a cross-section, respectively, with added Gaussian noise of variance 0.5.

The filtering process was performed as follows. First, the two-dimensional Fast Fourier Transform was used to convert the elevation data into spatial frequencies. Next, the 2D power spectrum was radially averaged to obtain vector versions of the power spectrum and the frequencies. A periodogram was then used to describe the frequency distribution of the elevation variance as a one-dimensional plot. This plot is inspected and two lines were manually fit: one for the estimated signal in the spectra, and for the estimate noise value (a horizontal line). The following diagram illustrates the manual fit

for the signal and noise equations in the log-log plot of the power spectrum in a synthetic landscape with added noise.

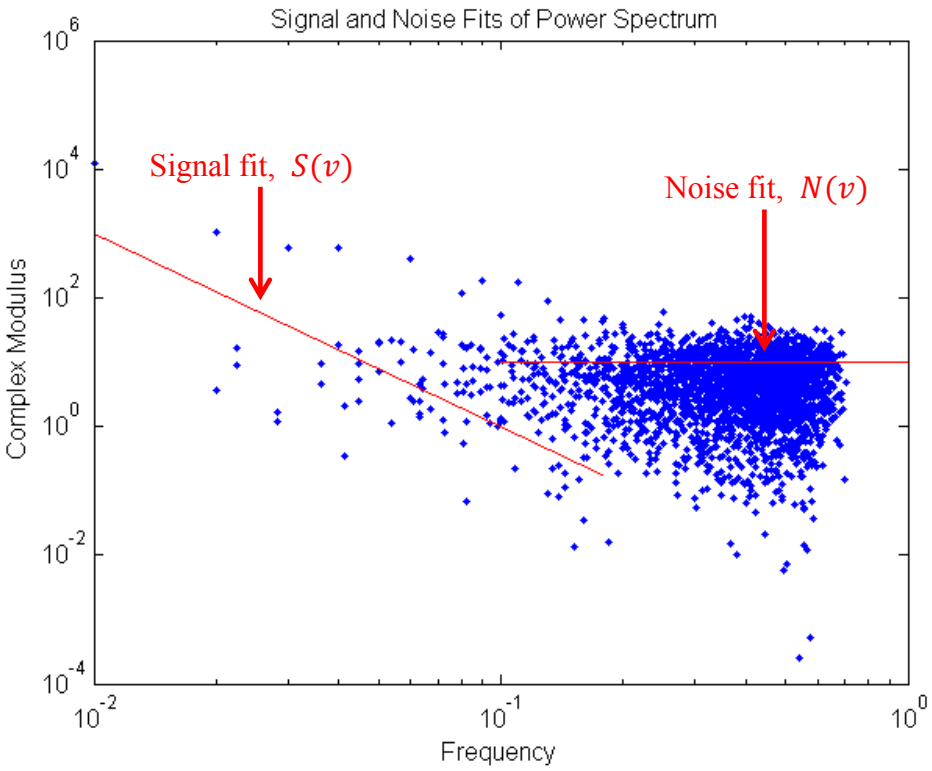


Figure 15: The red lines indicate the fits to the estimated signal and noise within the power spectrum for an idealized ridge with added noise. The equations for these lines are used to compose the transfer function, which attenuates the noise in the image.

The abundant scatter in the plot makes the noise and signal fits a subjective and iterative process. The noise value can be heightened and lowered, as well as the slope and intercept of the signal line be adjusted to optimize the appearance of the filtered image. For this analysis, the best fit of the signal and noise values was determined based on visual inspection of the filtered images in comparison with the original. Other methods of evaluation for the filter results are discussed later in this section.

After the equations for the signal and the noise were determined, a transfer function of spatial frequency, $\varphi(v)$, was composed. This expression is used to attenuate the noise in the spectra and is formulated for the OWF as the following:

$$\varphi(v) = \frac{|S(v)|^2}{|S(v)|^2 + |N(v)|^2} \tag{5.2.1}$$

Here, $S(v)$ is the equation of a line which fits the signal in the radially averaged spectra and $N(v)$ is the noise value fit. This transfer function was multiplied by the 2D array of spatial frequencies. When the noise values are very small, the transfer function is approximately unity and will not attenuate the frequency data. However, when more noise is present and the denominator of the transfer function becomes large, the transfer function value will decrease to less than unity, and begin to filter out the frequency data. Finally, the inverse Fast Fourier Transform was taken of the filtered frequency data in order to obtain a filtered image of the elevation data. As the identification of noise and signal in the power spectrum is not automatic and requires manual intervention, the use of the OWF in this analysis is an iterative process. The fits of the signal and noise lines were adjusted after several iterations to obtain the optimal filtered image based on visual inspection of the results after each test run.

The following images illustrate the difference between the two filters currently available in GeoNet: the Gaussian and Perona-Malik, and the OWF for the idealized ridge with added noise introduced in Figure 8. The results for the real landscapes are shown in the following section of this chapter.

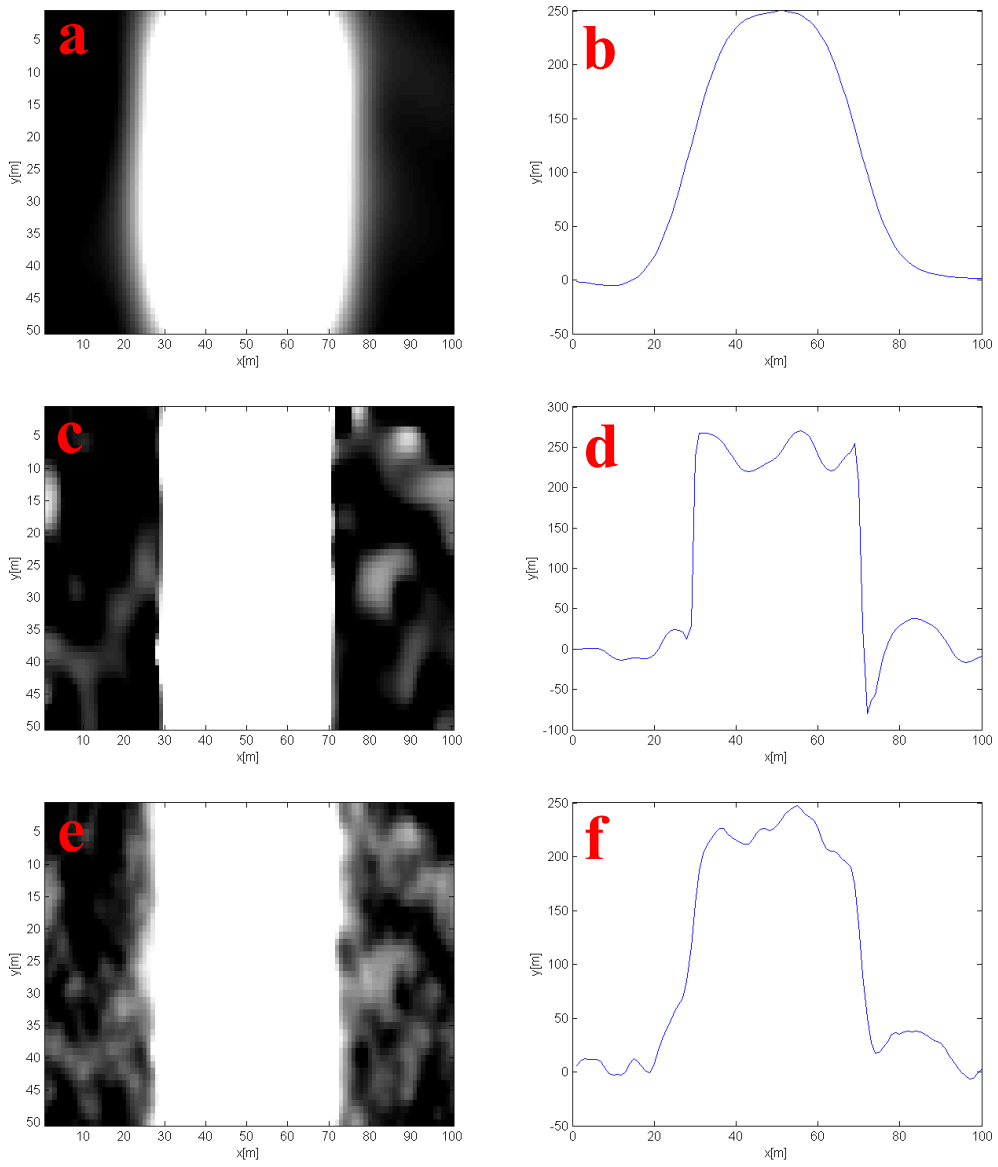


Figure 16: The Gaussian filtered ridge is shown in *a* and *b*. This linear filter smooths large-scale and small-noise noise at the same rate, and though the noise within the image is greatly reduced, it is reduced at the expense of the preservation of the ridge. The results of the filtered ridge using the Perona-Malik (with 50 iterations) in *c* and *d* . The noise is not completely removed but it is greatly reduced and the edges are maintained due to the edge-stopping function. The OWF results are shown in *e* and *f*. Again, the noise is not wholly reduced as in the Gaussian-filtered image but it is greatly reduced. The edges of the ridge are more maintained than the Gaussian results, but not as well as the Perona-Malik filtered results.

**Quantitative Comparison of Filters: The Correlation Coefficient**

As mentioned earlier in this section, the fits of the lines used to estimate the signal and noise in the spectra as based on visual inspection of the resulting filtered images. The "best fits" are those which result in a landscape in which small-scale elevation variability is reduced. However, in order to compare the OWF results with the Perona-Malik filtered results, a quantitative assessment of these differences between the original images and the filtered results provide further insights into the performance of each method.

*Mrazek & Navara* (2003) used the correlation coefficient to evaluate the effect of filters on intensity images. This is done by using the filtered image $h(t)$ as a proxy for the signal (for this study the signal is the elevation data to be preserved), and the absolute vale of the difference between the original image and the filtered image $h(0) - h(t)$ as a proxy for the noise (for this study the noise is the small-scale variability in the elevation data). The equation for the correlation coefficient between the signal and noise proxies is shown below:

$$corr\big(|h(0) - h(t)|, h(t)\big) = \frac{cov(|h(0) - h(t)|, h(t))}{\sqrt{var(|h(0) - h(t)| \cdot var\big(h(t)\big)}} \quad (5.2.2)$$

For the elevation data of an assumed relatively high quality in which the noise presence is small relative to the signal presence, when the correlation coefficient is minimized, the signal to noise ratio is maximized. In other words, increasingly negative values of correlation indicate the signal to be increasing while the noise decreases. For the OWF results, the correlation coefficient is calculated from the best fits to the signal and noise as determined by visual inspection of the filtered landscape.

## 3. STUDY SITES

Three of the study sites used in the assessment of the OWF were described in Chapter 4: Cascade Ridge, Piedmont, and Indian Creek. Additionally, the Tennessee Valley basin was used as a test case, and falls within the landscape type previously described as high relief (>250 m) and vegetative. The Tennessee Valley dataset lies within Marin County, California just north of San Francisco. This landscape features hillslopes of various scales and the vegetation is predominantly grasses [*Montgomery & Dietrich*, 1989].

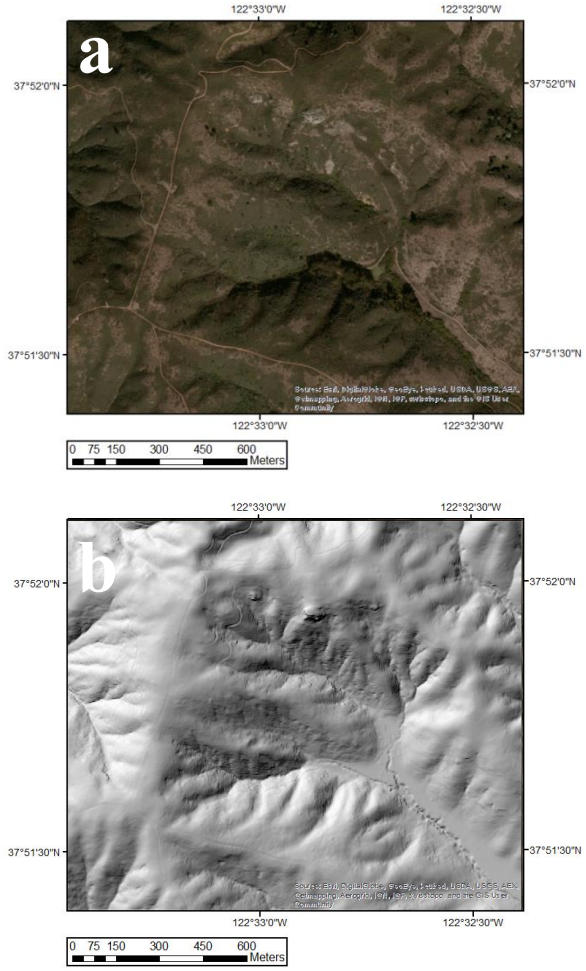


Figure 17. Image *a* shows satellite imagery of the Tennessee Valley site; *b* is the hillshade of the same extent.

## 4. RESULTS

This section compares the filtering capabilities of the OWF with the Perona-Malik filter in real landscapes without added noise. Challenges exist in comparing the OWF and the Perona-Malik as they operate in dissimilar manners; the Perona-Malik smooths and enhances the elevation data in a nonlinear way and requires a number of filtering iterations to be set, while the OWF is based on manual log-log fits of the signal and noise in the power spectrum for optimization. Two different methods of comparison are used here to provide a more comprehensive comparison of the OWF and Perona-Malik filtered results.

### Qualitative Comparison of Filtered Results

To begin, a visual comparison of results for a section of the Indian Creek landscape is given. A hillshade of the original DEM is shown first, followed by hillshades of the filtered landscapes using the Perona-Malik and OWF.

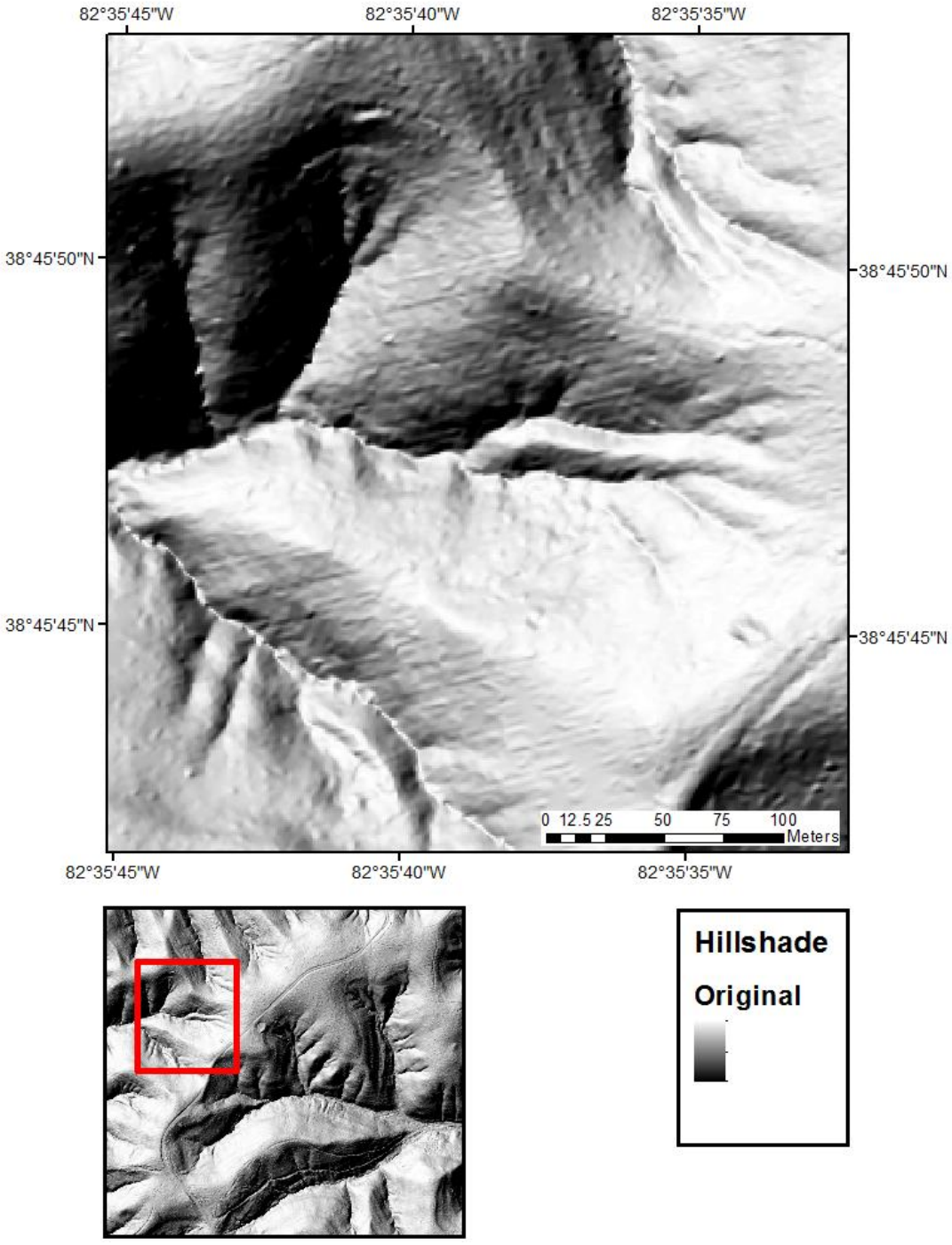


Figure 18: Hillshade of the original elevation data for Indian Creek.

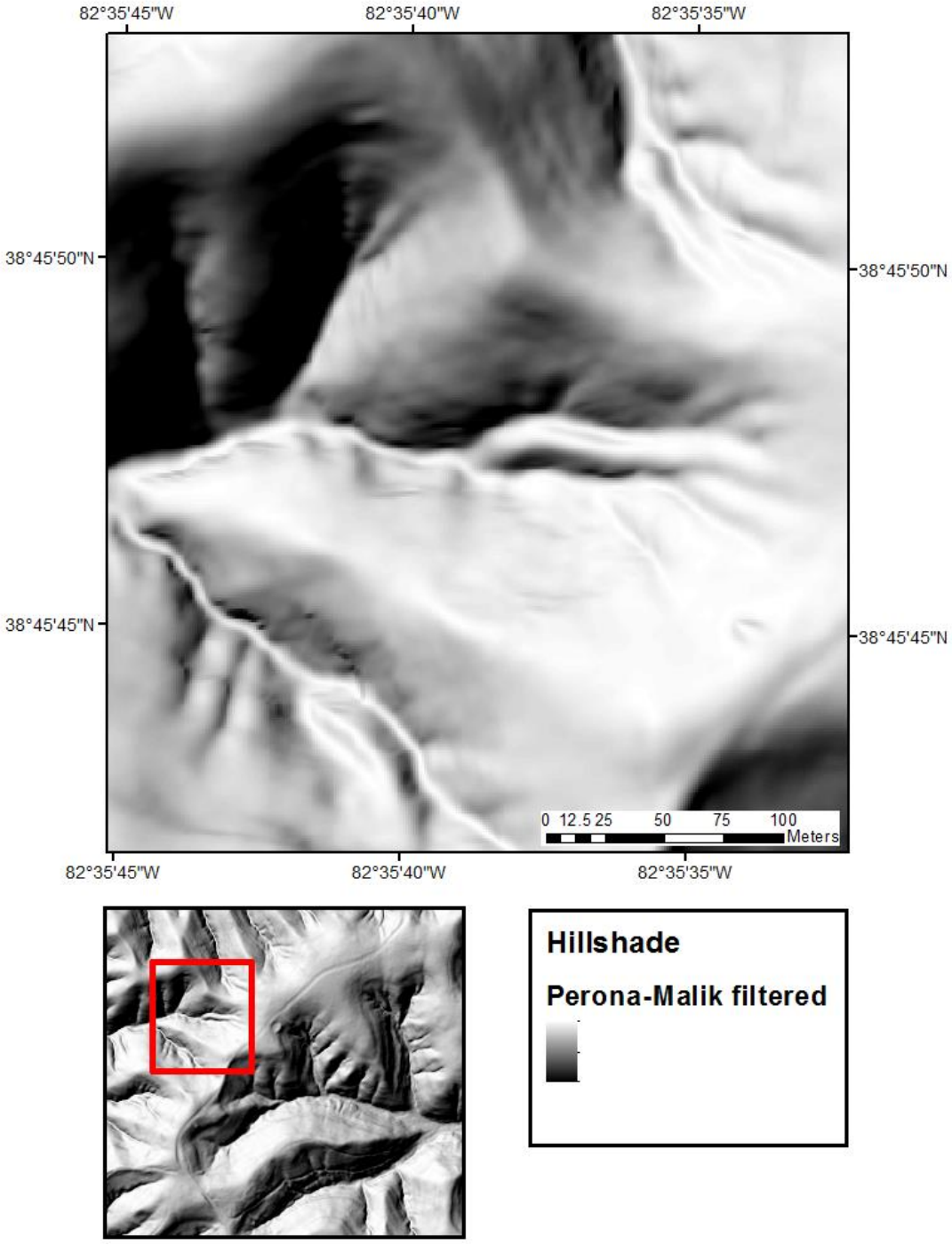


Figure 19: Hillshade of the Perona-Malik filtered DEM. Note the reduction in small-scale noise, yet the preservation of channel and ridge features.

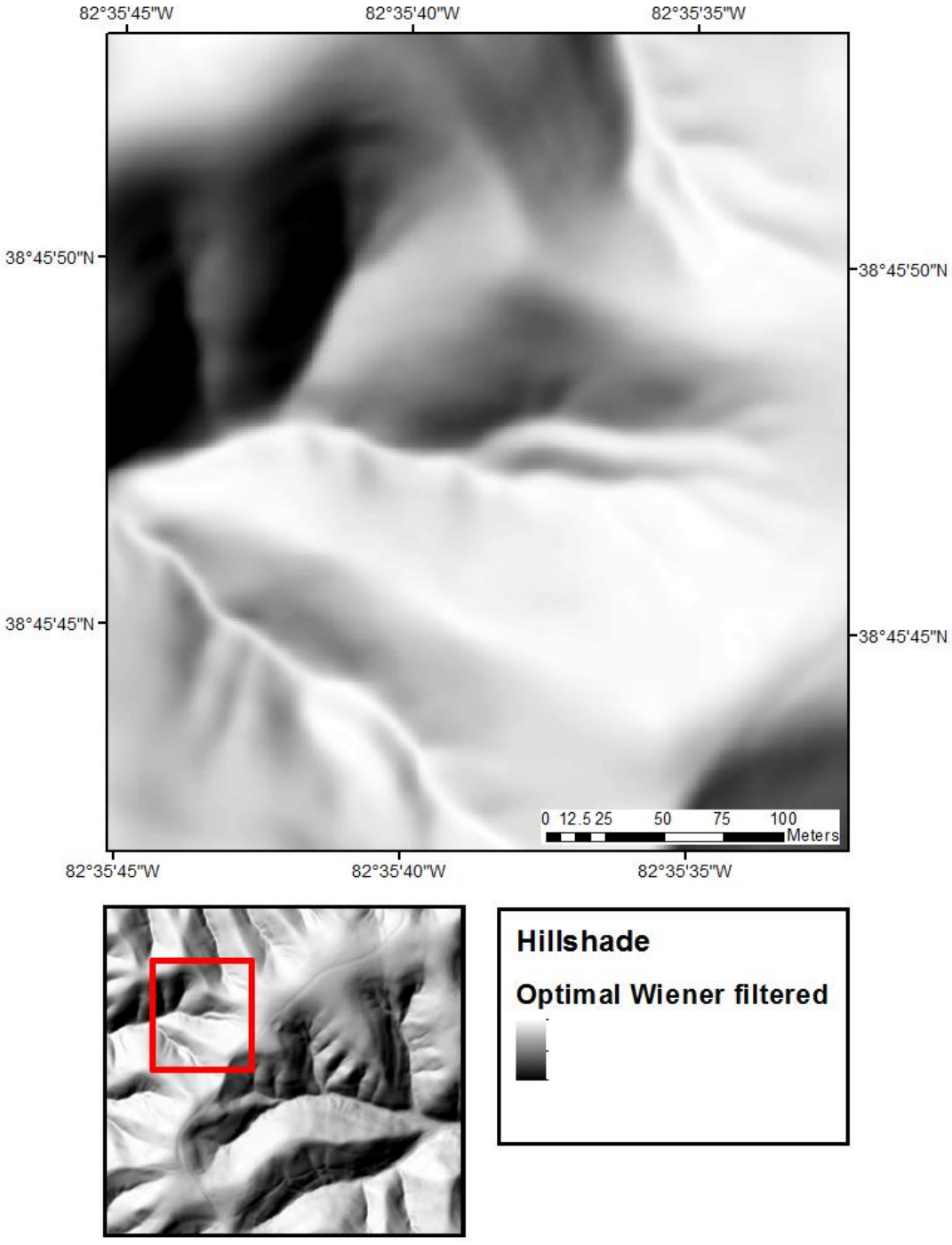


Figure 20: Hillshade of the Optimal Wiener filtered DEM. Note the overall reduction in noise, but the channel features are significantly more smoothed in comparison with the Perona-Malik filtered DEM hillshade.

## Quantitative Comparison of Filtered Results

For the Perona-Malik, the results are dependent on the number of iterations for the filter. *Sangireddy et al.* (in review) show the optimal number of filtering iterations can be obtained by plotting the correlation coefficients for successive iterations in accordance with the method proposed by *Mrazek & Navara* (2003). The correlation coefficients for different iterations are plotted for the four landscapes used in this analysis and shown below.

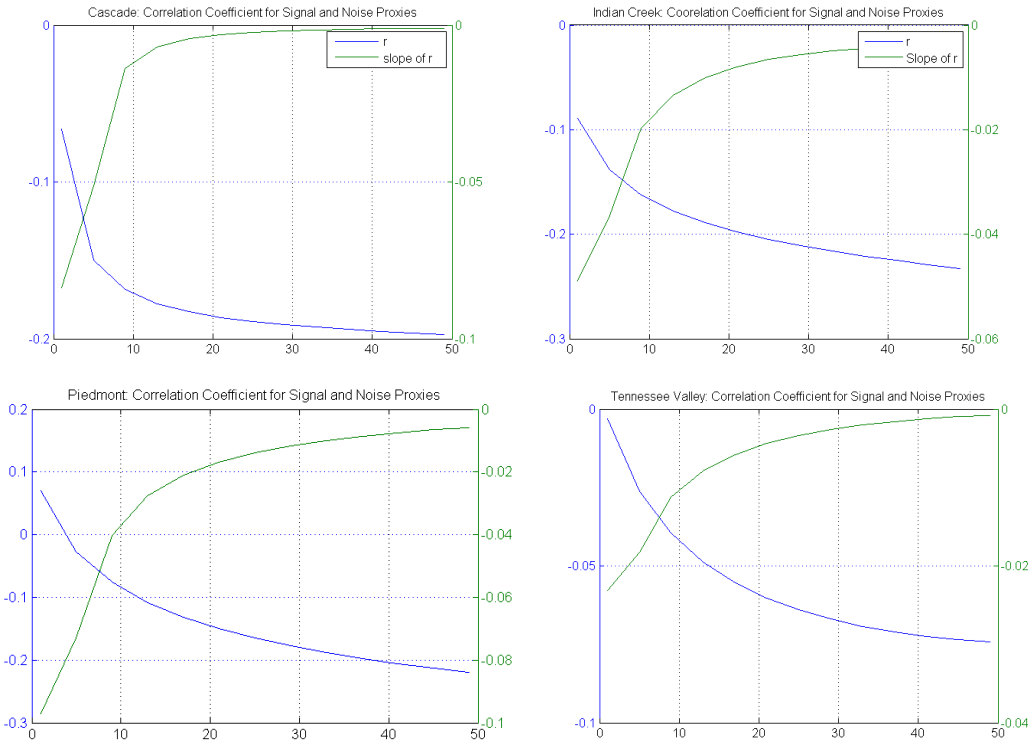


Figure 21: Correlation coefficients and the gradients thereof are plotted against the iterations for the Cascade Ridge, Indian Creek, Peidmont, and Tennessee Valley datasets.

The correlation coefficients for different iterations are plotted for the four landscapes used in this analysis and shown below. Based on these plots, the correlation coefficients are minimized and stable at approximately 50 iterations for all of the datasets. Therefore, this number of filtering iterations is used in the comparison with the OWF.

The correlation coefficient of the signal and noise proxies were calculated for OWF and the Perona-Malik filter at 50 iterations for the Cascade, Indian Creek, Piedmont, and Tennessee Valley datasets. The following table depicts those results.

| | | Dataset | | | |
|---|---|---|---|---|---|
| | | Cascade | Indian Creek | Piedmont | TN Valley |
| Correlation Coefficient | Perona-Malik | -0.1905 | -0.213 | -0.1642 | -0.1355 |
| | with OWF | 0.9003 | -0.1987 | -0.3173 | -0.1027 |

Table 1: Correlation coefficients between signal and noise proxies for Perona-Malik and OWF filtered results.

## 5. DISCUSSION

The OWF does reduce small scale variability in the landscape as shown in Figure 14 which depicts a detailed view of a channel section in the Indian Creek dataset. However, because the scale of the noise may be very close to the scale of some of the finer channel features, such as channel banks, these features appear to be smoothed as well. This is more apparent in comparison with the Perona-Malik results (Figure 19) in which the channel banks are still identifiable though the noise is reduced. The correlation coefficients shown in Table 1 describe the quantitative difference between the Perona-Malik and OWF filter results. As described in the Methods section, the lower correlation

coefficient indicates a higher signal to noise ratio. This table shows Perona-Malik performs much better in the Cascade dataset, and only slightly better in the Indian Creek and Tennessee Valley sites. The OWF has a lower correlation coefficient in the Piedmont site. The results indicate that the Perona-Malik performs slightly better than the OWF on real landscapes, but the variability in these values indicates more datasets should be experimented on in order to substantiate that assertion.

This filtering method has previously been tested on synthetic landscapes with added Gaussian noise, but in real landscapes the utility of the OWF is questionable. Furthermore, the lack of automation in the line-fitting portion of the OWF restricts the introduction of this filtering option in the GeoNet framework. Though these results indicate that the Perona-Malik is the optimal filtering option for channel feature extraction of the two, further work should be conducted in order to see if these fits of the spectral signal and noise can be optimized and automated with better results.

# Chapter 6: Urban Flow Paths

## 1. OBJECTIVE

***Assess the performance of GeoNet in urban landscapes and make recommendations for users and future development***

## 2. METHODS

### MatLab-based GeoNet

This research was the first application of GeoNet in an urban landscape. The methodology was employed for the urban hydrologic context in two ways: an adapted version of the MatLab-based algorithm, and the Python-based GeoNet algorithm. The MatLab-based GeoNet algorithm was edited so that a mask of building footprints (shown in the third section of this chapter) is read-in during the processing. The purpose of this was to distinguish the buildings from the urban landscape so flow paths did not cross over or begin on the buildings. The buildings were idealized as isolated portions of the landscape. Pixels corresponding to buildings were treated in two different ways during the processing. Building pixels were as NaNs for the computation of slope and curvature, so that they were not identified as highly convergent features. However, building pixels must have elevation values for the flow routing procedure in order for flow to be routed around and not through the buildings. During the flow routing, the elevation values for the building pixels were set to the highest elevation value in the dataset. Thereby flow routing was continuous throughout the landscape but circumvented the buildings.

In the MatLab-based approach a low pass median filter was used prior to the Perona-Malik filter. The median filter operates such that a window moves across the image and sets the elevation value of the centroid pixel in the window to the median

elevation value within the window. The edge size of this window is set by the user before running the algorithm and several window sizes were tested in this study. *Hughes et al.* (2004) suggested setting the window edge size to the average road width in the study area, which for the urban dataset used here is approximately 16 meters. This coupled filtering method was recently developed and released in the latest version of GeoNet *Sangireddy et al.* (in review). The authors found the combination of the low pass median and Perona-Malik filters more successfully minimized small-scale anthropogenic noise in the landscape, in comparison with the use of the Perona-Malik alone. *Sangireddy et al.* (in review) also recommend a median filter size of 2-3 times the road width. For this analysis median filters of size 16, 32, and 48 meters were used.

Another difference in the MatLab-based urban analysis was the use of geometric curvature computation method instead of the Laplacian which is typically recommended for landscapes with natural and engineered features [*Passalacqua et al.* (2012)]. The rationale for this is the use of the combination of the building mask, and median and Perona-Malik filters strips the urban landscape of anthropogenic features leaving essentially only "natural" features, and therefore the selective nature (in terms of convergent features) of the Laplacian computation method is not necessary.

**Python-based GeoNet**

The Python-based GeoNet version was also tested on the same urban site using the Perona-Malik filtering operation coupled with the Laplacian curvature calculation method, which is typically recommended for this type of landscape as mentioned earlier. The Python-based GeoNet does not yet include the building mask process as described for the MatLab-based version. The dataset was also run in Python-based GeoNet at 0.3 meter scale (lidar was acquired at one foot resolution). Python-based GeoNet uses a

multi-directional flow routing through GRASS GIS, which makes it more robust for handling large datasets.

For both MatLab-based and Python-based GeoNet, the flow accumulation area threshold was set to 1300 square meters. As no field work was collected to ascertain an estimate of source area, this value was obtained by trial and error after examination of the channel network and end point results.

### Field Work

Field work was conducted on two occasions to observe urban flow paths within the study site during non-storm conditions and during an intense precipitation event. This work was carried out on April 16$^{th}$ and 17$^{th}$ of 2015. This work included taking photos and video of a culvert crossing Walnut Creek and the surrounding area, as well as the measuring of flow path width during a storm event.

## 3. Study Sites & Data

The urban landscape examined here is within the city of Austin and is of low relief (<50 m), and presents engineered features including buildings, roads, irrigation canals, as well as a partially modified natural channel, Walnut Creek. This dataset is from a Travis County-wide lidar scan taken at a foot-scale resolution. DEMs were created from the point cloud using the ESRI lidar tools at ~0.3 m (1 foot) resolution and at 1 meter resolution.


Figure 22: Image *a* shows satellite imagery of the Walnut Creek site; *b* is the hillshade of the same extent.

The building footprint dataset used to create the building mask was obtained from the City of Austin GIS website. The mask over the hillshade of the dataset is shown in the following figure.

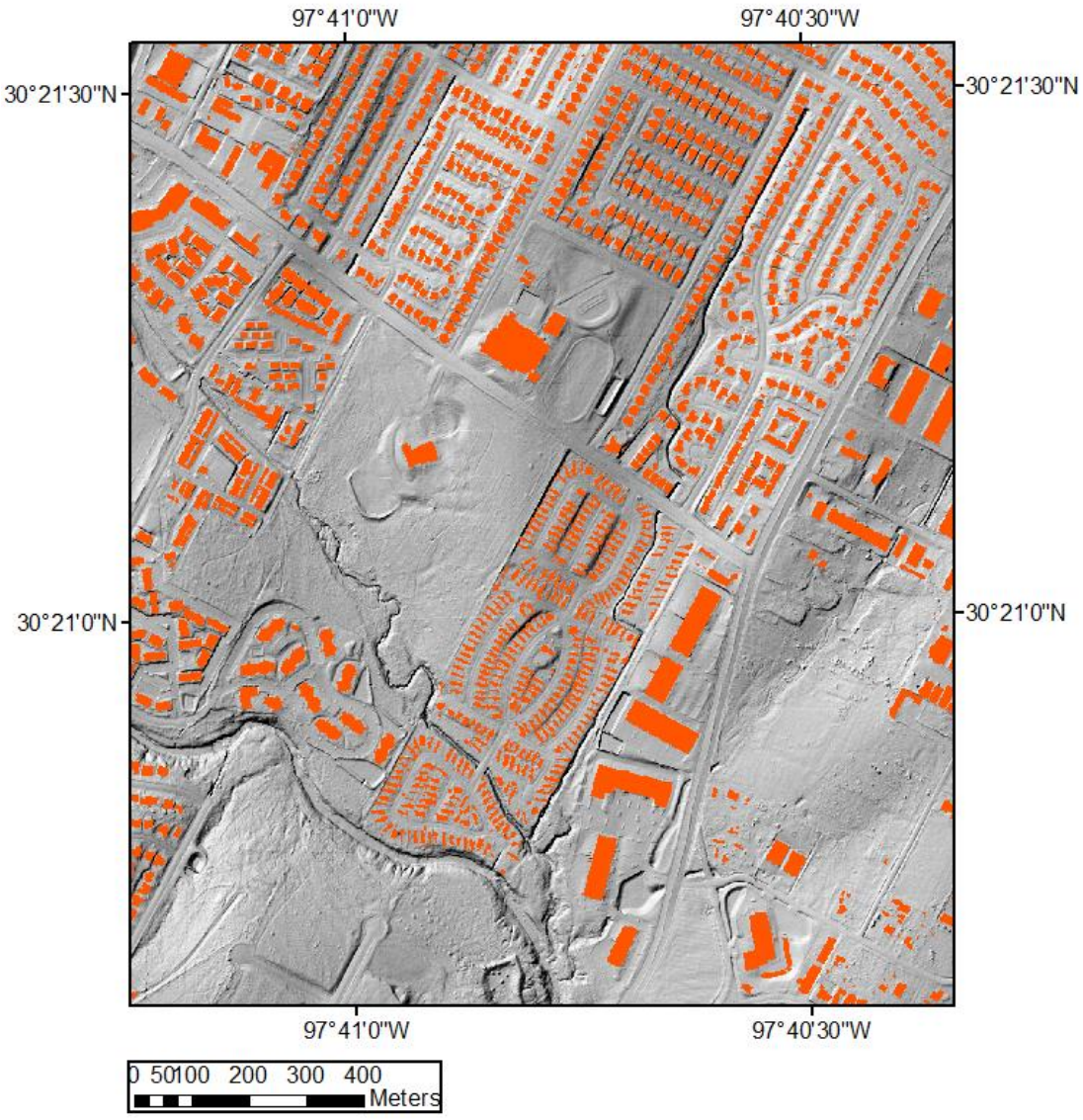


Figure 23: Overlay of building footprint mask with hillshade of Walnut Creek data.

## 4. RESULTS

The channel skeleton results (.tifs) depict the urban flow path estimates in Walnut Creek. From the MatLab-based GeoNet results, maps showing the channel network skeleton using each of the three median filter sizes are shown in the following figures.

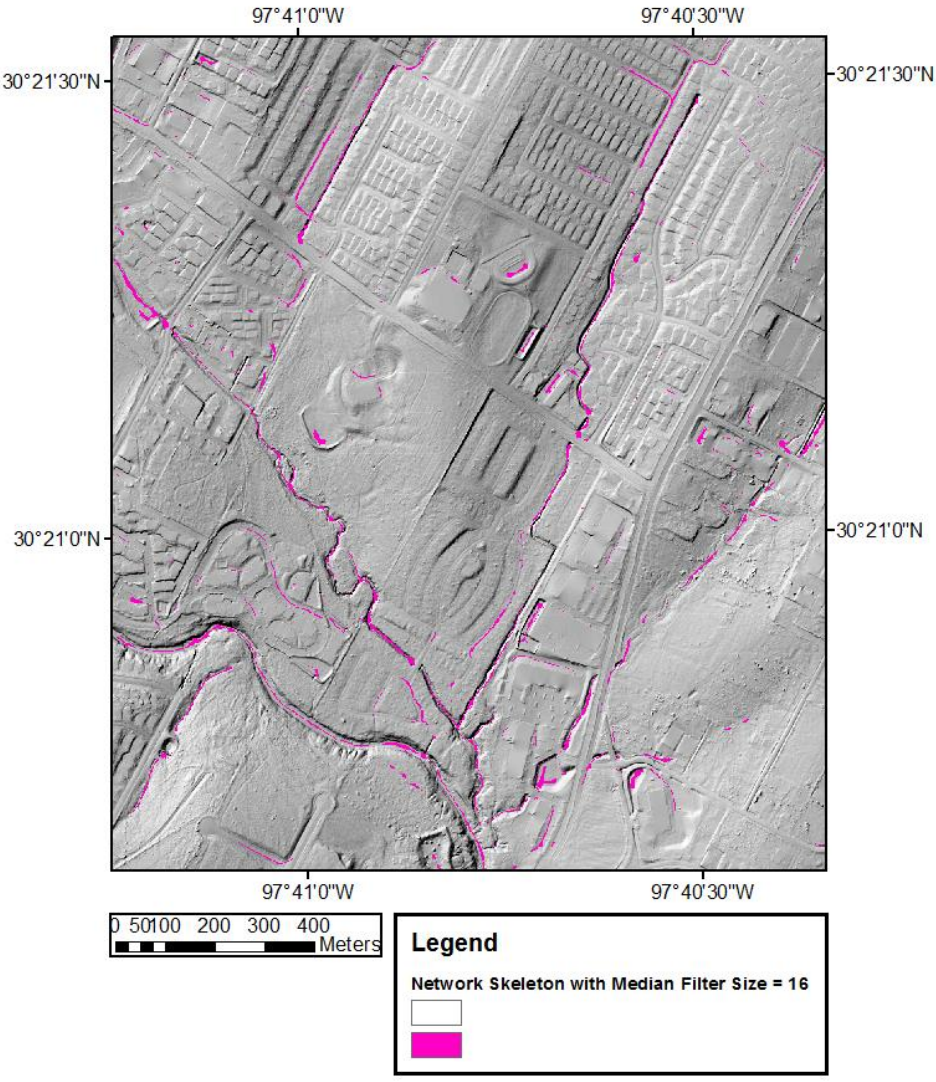


Figure 24: MatLab-based channel skeleton with median filter size of 16 m overlaid on hillshade of Walnut Creek data.

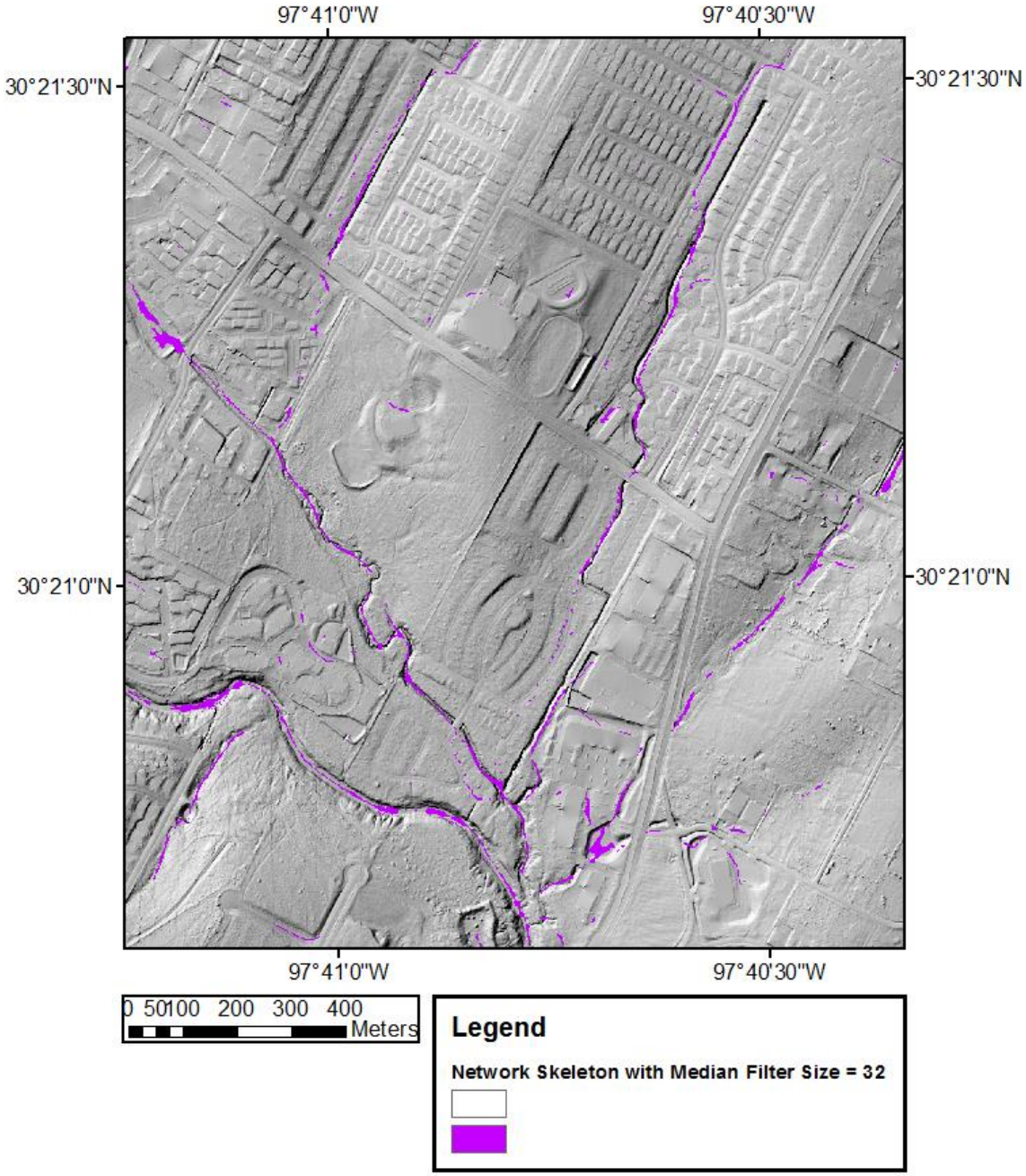


Figure 25: MatLab-based channel skeleton with median filter size of 32 m overlaid on hillshade of Walnut Creek data.

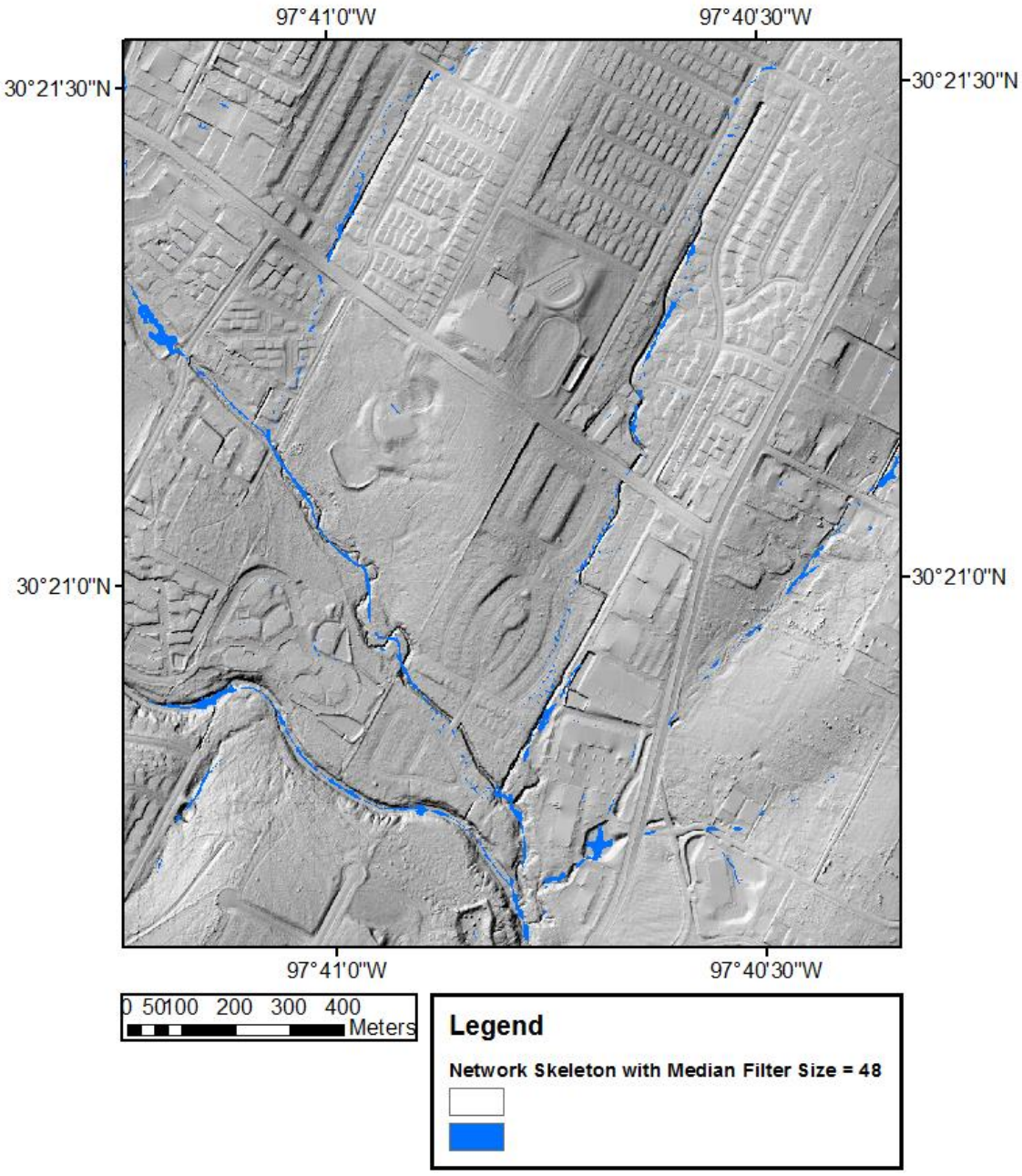


Figure 26: MatLab-based channel skeleton with median filter size of 48 m overlaid on hillshade of Walnut Creek data.

For the Python-based GeoNet runs on the 1 meter resolution DEM, the channel skeleton results using the Laplacian and geometric curvature results are shown below.

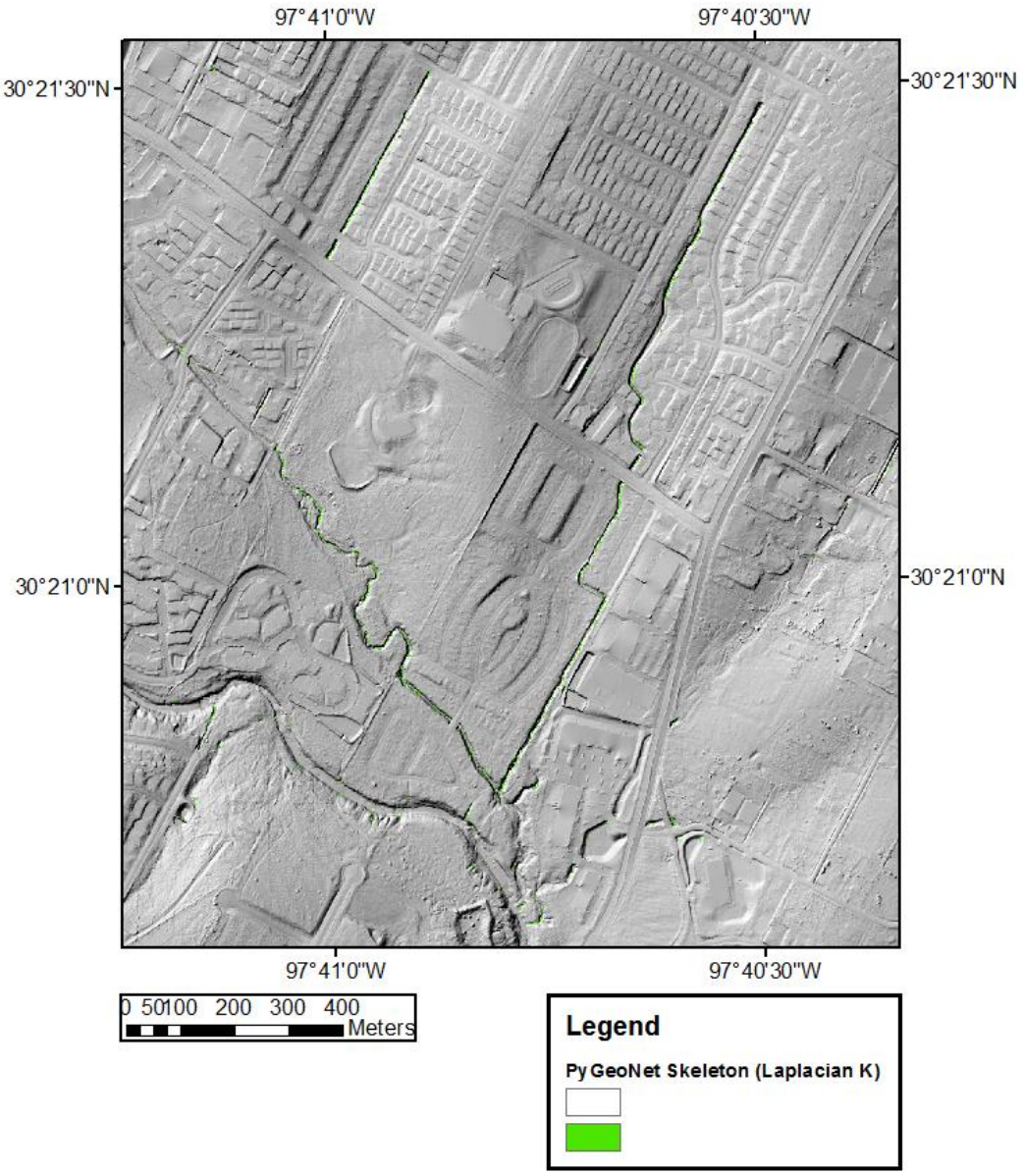


Figure 27: Python-based GeoNet channel skeleton for 1 meter resolution DEM with Laplacian curvature method overlaid on hillshade of Walnut Creek data.

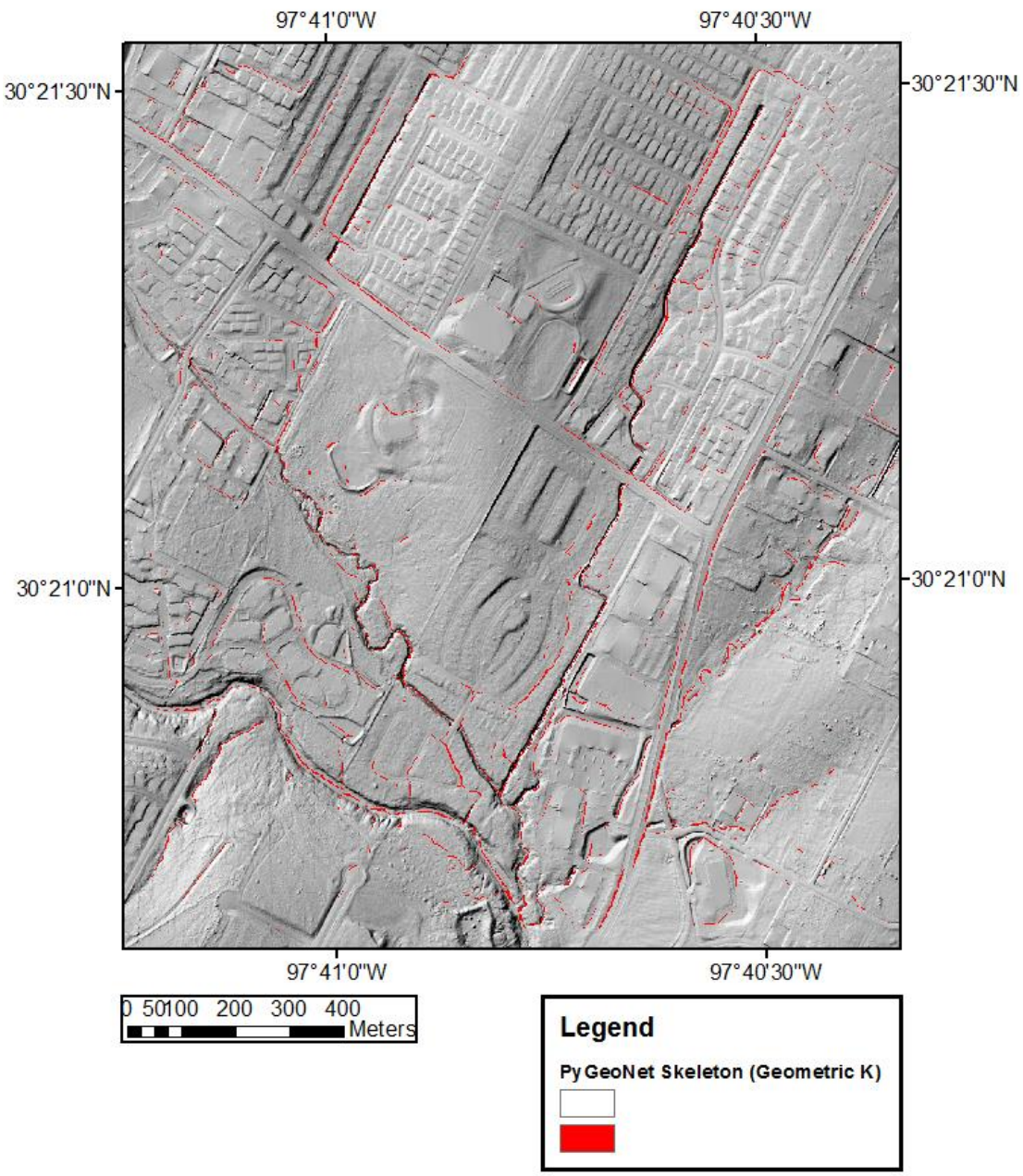


Figure 28: Python-based GeoNet channel skeleton for 1 meter resolution DEM with geometric curvature method overlaid on hillshade of Walnut Creek data.

For the Python-based GeoNet runs on the 0.3 meter resolution DEM, the results for both the geometric and Laplacian curvature results are shown in the following two figures.

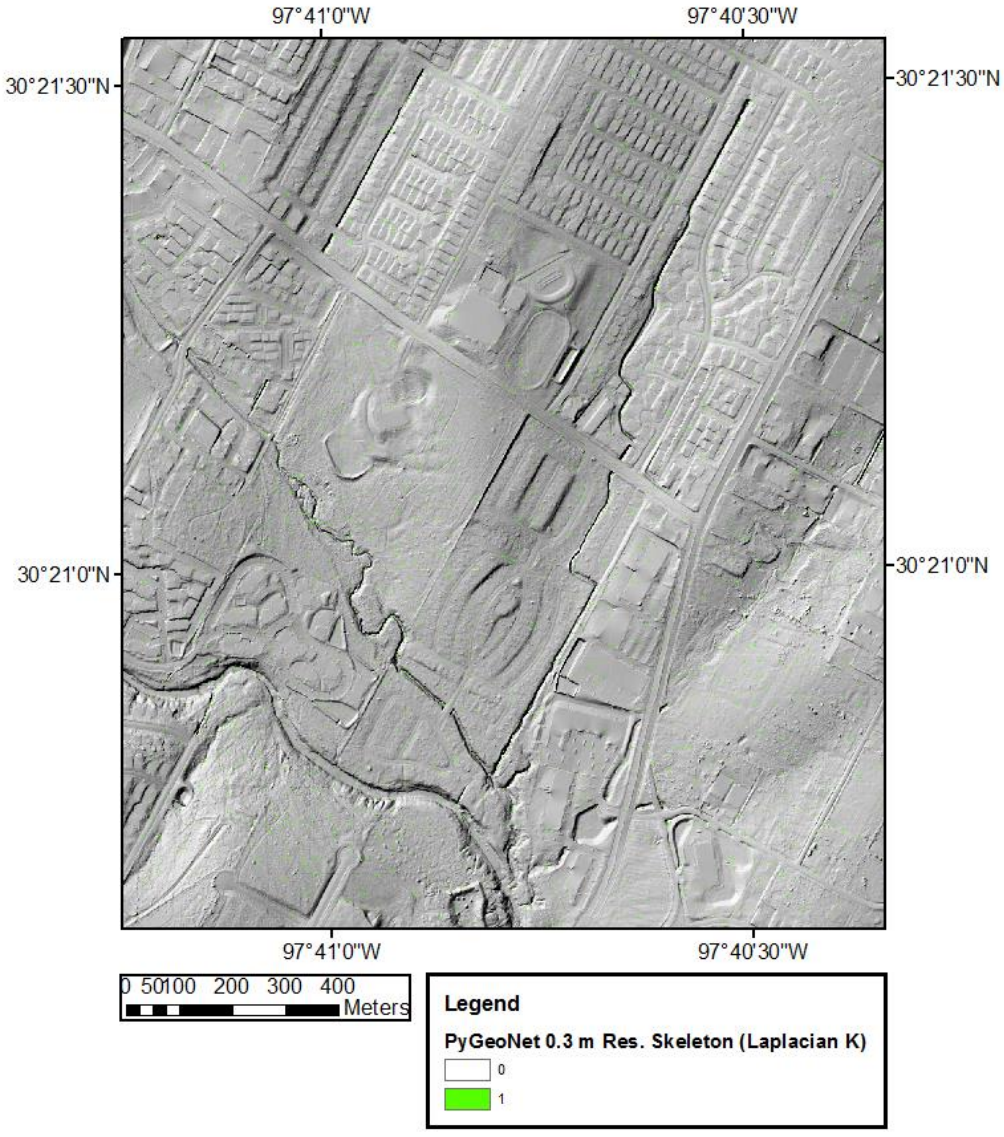


Figure 29: Python-based GeoNet channel skeleton for 0.3 meter resolution DEM with Laplacian curvature method overlaid on hillshade of Walnut Creek data.

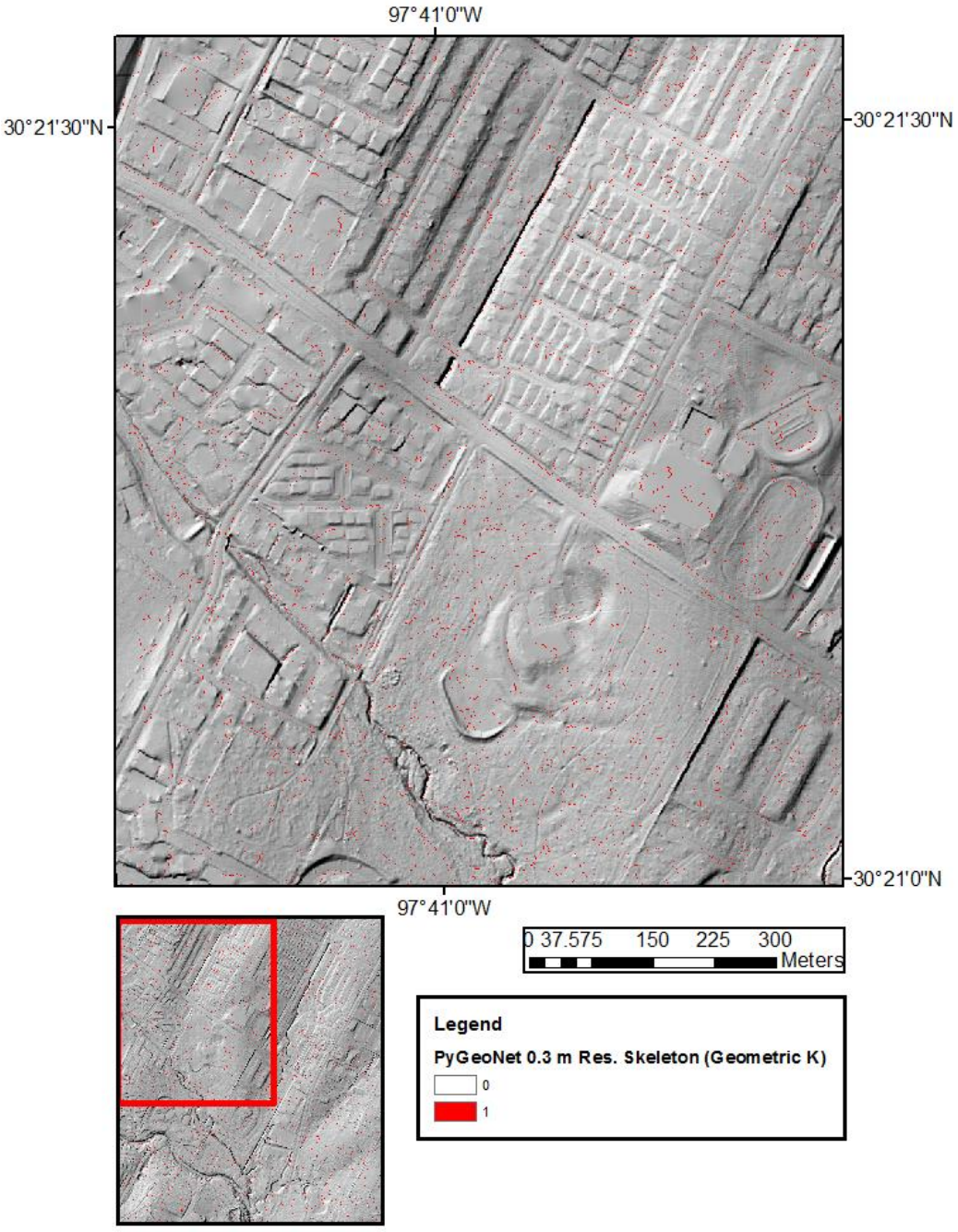


Figure 30: Python-based GeoNet channel skeleton for 0.3 meter resolution DEM with geometric curvature method overlaid on hillshade of Walnut Creek data.

## 5. DISCUSSION

The results from the MatLab-based version of GeoNet indicate that a median filter window size of three times the road width is optimal in comparison with sizes equal to the road width and two times the road width. A comparison of Figures 24, 25, and 26 in the previous section indicate that as the window size increases, less of the roads are integrated into the flow path network, while stream features and artificially altered canals are maintained. However, for urban flooding applications it may be advantageous to also map out likely channelized connectivity between affirmed urban channel networks and ephemeral flow paths.

For the Python-based GeoNet results for the 1 meter resolution data, the Laplacian curvature computation method performs better than the geometric. There are far more disconnected road features identified in the skeleton in Figure 28 (geometric) than in Figure 27 (Laplacian), which is in agreement with previous research using the Laplacian in low relief landscapes with engineered features [*Passalacqua et al.*, 2012]. The channel results for the Laplacian curvature computation method do not cross through any buildings within the dataset, even without the use of a building mask. However, there is some crossover of the channel network through the buildings using the geometric curvature computation method, as show in the following figure.

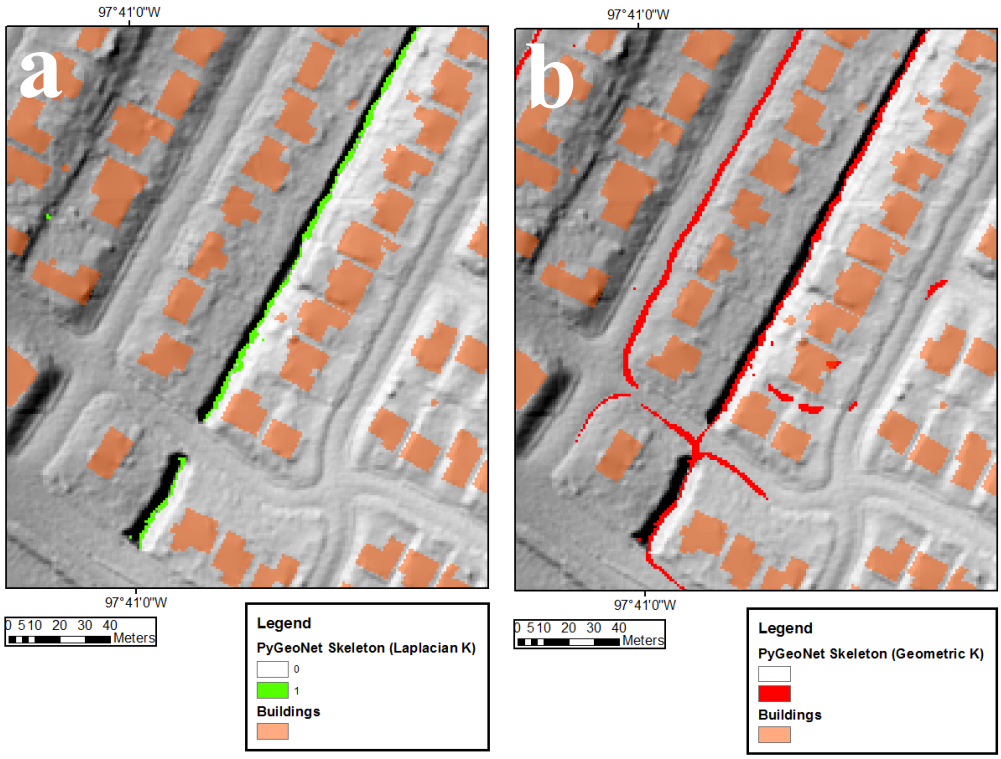


Figure 31: Python-based GeoNet channel skeletons for the 1 m resolution data using the Laplacian (*a*) and geometric (*b*) curvature computation methods. In *b* there are some locations were the channel network crosses through the buildings.

Surprisingly, the higher resolution imagery (0.3 m) does not translate into improved estimate of the urban flow paths as shown in Figures 29 and 30. These results indicate that higher resolution data (< 1 meter) may not be appropriate for analyzing a dataset of this extent, and may be more suitable for a study of finer scale urban features, such as culverts and narrow drainage paths in a smaller area. Moreover, these results confirm an 'optimal' scale exists for curvature calculation used for larger scale features such as channels and roads in accordance with previous studies [*Sofia et al.*, 2011; *Tarolli et al.*, 2012].

The following figure depicts the two areas which were the focus of the field work. The map with the MatLab-based flow path skeleton results for the 48 m median is shown for reference. Site *a* is in the northern section of the map, an engineered channel lined with concrete and approximately 2.4 m wide lies between two rows of houses. Site *a* is in the southwestern section of the map, a culvert on Fiskville Cemetery Road crosses a portion of Walnut Creek near several residential areas, a wooded area, and a cemetery.

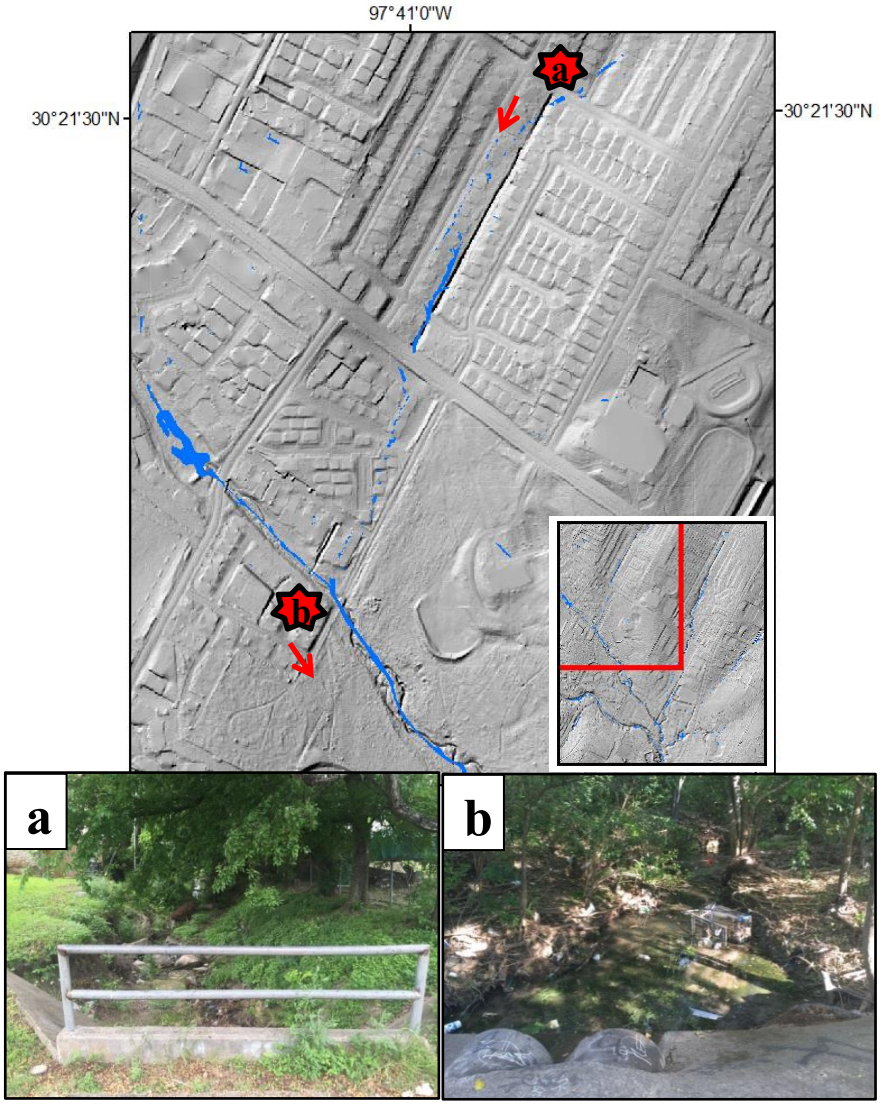


Figure 32: Field site locations indicated in the map of the Walnut Creek dataset. The arrow direction for each site indicates the view shown from each photo. Site *a* is the upstream portion of an engineered canal. Site *b* is focused on a culvert which crosses a portion of Walnut Creek; the view shown in the photo is looking downstream into a wooded, non-residential area.

The comparison of the optimal MatLab-based and Python-based GeoNet results (median filter of size 48 m and Laplacian curvature respectively; Figure 26 and 27), indicate both methods adequately identified the channel feature in both sites, and both connected the channel over the culvert on Fiskville Cemetery Road. There are differences between the results; downstream of and at location *a* the Python-based GeoNet method has a more precise skeleton result and clearly identified the engineered canal and most upstream location, whereas the MatLab-based skeleton results depicted a more variable flow path which extends beyond the upstream extent of the canal. However, the MatLab-based skeleton results a provide a more detailed depiction of the meandering nature of the flow path upstream of the culvert at Fiskville Cemetery Road indicated in the following figure with a yellow star.

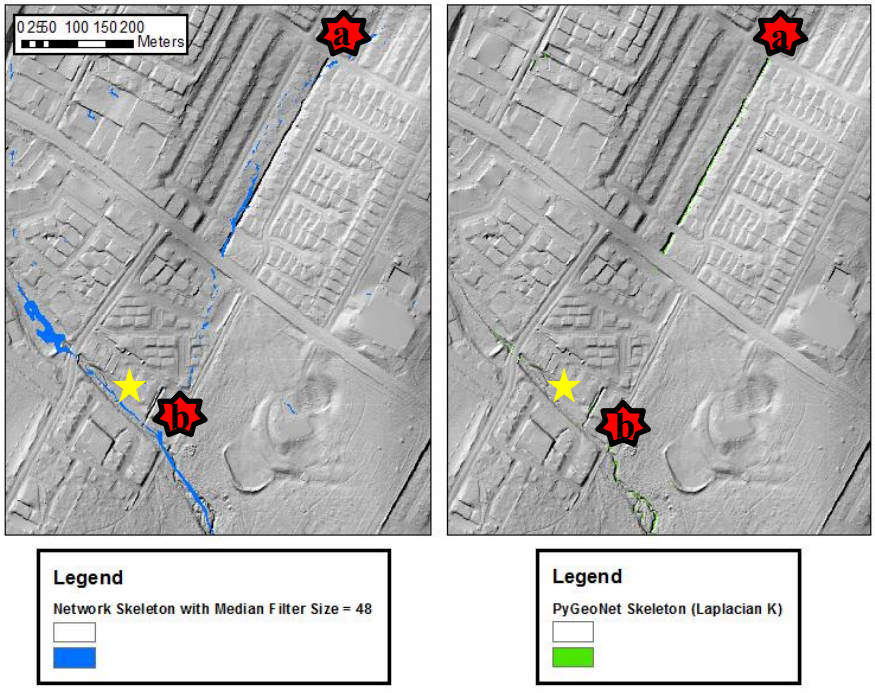


Figure 33: Field site locations indicated in the map of the Walnut Creek dataset with the MatLab-based (blue) and Python-based GeoNet (green) skeletons. The gold star corresponds to the meandering location upstream of the culvert.

Figure 34: These photos show the meandering features of Walnut Creek upstream of the culvert on Fiskville Cemetery Road. The gold star in Figure 25 corresponds to this location.

The differences between these results can be attributed to the differences in the curvature computation method. The geometric curvature is normalized by the gradient as shown in Equation 3.6 and thus makes areas with small or large curvature values equally detectable. The geometric is known to perform better in natural landscapes [*Passalacqua et al.*, 2010b], which explains why the meandering flow path upstream of the culvert is more clearly identified in that skeleton. As mentioned previously, the Laplacian curvature computation is a more selective identifier of convergent features, which can be attributed to the more distinct flow path in the engineered canal. These findings demonstrate the usefulness and insights field work provides in the validation of these methods.

# Chapter 7: Discussion & Conclusions

## EVALUATION OF NEW METHODS TESTED

GeoNet is an open-source feature extraction algorithm and a key aspect to the continual improvement of the framework and expansion of the capabilities thereof is responsiveness to method development in the research community. Recent methods proposed by researchers include the use of a contour curvature threshold as a filtering method for spurious channel heads, as well as the use of the Optimal Wiener filter (OWF) to eliminate small-scale topographic noise in lidar-derived DEMs [*Pelletier*, 2013; *Clubb et al.*, 2014].

The contour curvature method was tested in this study on the same landscapes used in the *Clubb et al.* (2014) study. As the results show in Chapter 4, some channel end points did have contour curvature values greater than the threshold, but others did not. The particular utility for the use of this method in the GeoNet framework would have been a reduction in channel end points estimated within the downstream portion of the channel bed. For all landscapes evaluated in this study, there were end points estimated in the downstream regions with contour curvature values greater than the threshold (Figures 6-13). At this time, the contour curvature method will not be introduced into the GeoNet framework.

Spectral analysis has become more widely used to examine the spatial frequencies of landscape features and topographic noise [*Perron et al.*, 2008; *Booth et al.*, 2009; *Pelletier*, 2013]. The OWF was tested on four real landscapes in this study and the filtered results were compared to those of the Perona-Malik both visually and quantitatively via the correlation coefficient. The visual comparison of the OWF and Perona-Malik indicate the OWF filters out important small-scale channel features (e.g. banks), whereas the Perona-Malik preserves them. However, further work is necessary to

optimize the signal and noise line-fitting process, which may result in improved OWF performance. The manual aspects of the current OWF procedure also prohibit its inclusion in GeoNet at this time.

### RECOMMENDATIONS FOR URBAN FLOW PATH ANALYSIS

Both the MatLab-based and the Python-based GeoNet versions successfully extracted urban flow paths in the Walnut Creek dataset. For MatLab users, a median filter size of 3 times the road width (in meters) is recommended, coupled with the geometric curvature method. For Python users (which is also recommended if building footprint data is unavailable), the Laplacian curvature method is recommended. The differences between the extracted channels result from the curvature computation type; the geometric curvature more fully identifies natural channel features in the urban landscape, whereas using the Laplacian curvature more clearly identifies engineered channel features.

The results for the 0.3 m resolution dataset indicate that for a dataset of the size of Walnut Creek and of fine resolution, the algorithm identifies very small convergent features and the skeleton results are not improved compared to the 1 m resolution skeleton results. The scale at which the curvature is calculated impacts the results in that very small convergent areas are identified while the convergence that composes the entire channel is not. Future work is need to assess whether a fine scale analysis of smaller data extents will provide insights into fine, ephemeral urban flow paths which may have applications in the design of urban roadways, culverts and drainage schemes.

### FINAL REMARKS

High resolution topography data promises many exciting opportunities to validate and improve feature extraction methodologies, especially when coupled with field collected data. The use of field surveyed information for the landscapes studied in this

report was an invaluable tool for validation of the algorithm and improved understanding of the mass and energy transport processes at work in each location. As point cloud data acquisition technologies become more widely used and more economical, the likelihood of repeated data collection will become more feasible, which would allow more thorough monitoring of changes in channel structures in both natural and urban landscapes [*Passalacqua et al.*, 2014]. Expanded field work that couples traditional methods and high resolution imagery analysis will lead to improved models of fluvial phenomena in diverse settings and prompt advancements in water resource planning and management.

# References


Bates, P.D. , M.S. Horritt & T.J. Fewtrell. (2010). A simple inertial formulation of the shallow water equations for efficient two-dimensional flood inundation modelling. *Journal of Hydrology*, *387*(1-2), 33–45.

Booth, A.M., J.J. Roering & J.T. Perron. (2009). Automated landslide mapping using spectral analysis and high-resolution topographic data: Puget Sound lowlands, Washington, and Portland Hills, Oregon. *Geomorphology*, *109*, 132–147.

Cazorzi, F., G. Dalla Fontana, A. De Luca, G. Sofia & P. Tarolli. (2013). Drainage network detection and assessment of network storage capacity in agrarian landscape. *Hydrol. Process., 27,* 541–553. doi: 10.1002/hyp.9224.

Clubb, F.J., S.M. Mudd, D.T. Milodowski, M.D. Hurst, & L.J. Slater. (2014). Objective extraction of channel heads from high-resolution topographic data. *Water Resources Research, 50*(5), 4283-4304. doi: 10.1002/2013WR015167.

Dietrich, W.E., C.J. Wilson, D.R. Montgomery, & J. McKean. (1993). Analysis of erosion thresholds, channel networks, and landscape morphology using a digital terrain model. *The Journal of Geology*, *101*(2), 259-278.

Giannoni, F., G. Roth, & R. Rudari. (2005). A procedure for drainage network identification from geomorphology and its application to the prediction of the hydrologic response. *Advances in Water Resources*, *28*(6), 567–581.

Horton, R.E. (1945). Erosional development of streams and their drainage basins: hydrophysical approach to quantitative geomorphology. *Bulletin of the Geological Society of America*, *56*, 275-370.

Hudak, A. T., J. S. Evans, & A. M. S. Smith. (2009) Review: LiDAR utility for natural resource managers. *Remote Sensing*, *1*, 934–951. doi:10.3390/rs1040934.

Hughes, W. E., K. Eccles, D. Harwood, I. Potts & E. Hauer. (2004). Development of a Highway Safety Manual. No. 286. Transportation Research Board.

Hyde, K. D., A. C.Wilcox, K. Jencsoc, & S. Woods. (2014). Effects of vegetation disturbance by fire on channel initiation thresholds. *Geomorphology*, *214*, 84–96. doi:10.1016/j.geomorph.2014.03.013.

Jaboyedoff, M., T.Oppikofer, A. Abellán, M.H. Derron, A. Loye, R. Metzger & A. Pedrazzini. (2010). Use of LIDAR in landslide investigations: a review. *Natural Hazards*, *61*(1), 5-28. doi: 10.1007/s11069-010-9634-2.

Julian, J. P., A. J. Elmore, & S. M. Guinn. (2012). Channel head locations in forested watersheds across the mid-Atlantic United States: A physiographic analysis, *Geomorphology*, *177–178*, 194–203. doi:10.1016/j.geomorph.2012.07.029.

Lashermes, B., E. Foufoula-Georgiou, & W. E. Dietrich. (2007). Channel network extraction from high resolution topography using wavelets. *Geophysical Research Letters, 34*(L23S04). doi:10.1029/2007GL031140.

Meesuk, V., Z. Vojinovic , A. E. Mynett, & A. F. Abdullah. (2015). Urban flood modelling combining top-view LiDAR data with ground-view SfM observations. *Advances in Water Resources*, *75*, 105-117. doi:10.1016/j.advwatres.2014.11.008

Mitasova, H., & J. Hofierka. (1993). Interpolation by regularized spline with tension: II. application to terrain modeling and surface geometry analysis. *Mathematical Geology*, *25*, 657-669.

Montgomery, D.R. & W.E. Dietrich. (1988). Where do channels begin? *Nature*, *336*, 232-234. doi:10.1038/336232a0.

Montgomery, D.R. & E. Foufoula-Georgiou. (1993). Channel network source representation using digital elevation models. *Water Resources Research*, *29*(12), 3925-3934.

Mrazek, P. & M. Navara. (2003). Selection of optimal stopping time for nonlinear diffusion filtering. *International Journal of Computer Vision*, *52*(2-3), 189-203.

Passalacqua, P., T.D. Trung, E. Foufoula-Georgiou, & W.E. Dietrich. (2010a). A geometric framework for channel network extraction from lidar: Nonlinear diffusion and geodesic paths. *Journal of Geophysical Research*, *115*(F01002). doi: 10.1177/030913338000400204.

Passalacqua, P., P. Tarolli, & E. Foufoula-Georgiou. (2010b). Testing spacescale methodologies for automatic geomorphic feature extraction from lidar in a complex mountainous landscape. *Water Resources Research*, *46*(W11535). doi: 10.1029/2009WR008812.

Passalacqua, P., P. Belmont, & E. Foufoula-Georgiou. (2012). Automatic geomorphic feature extraction from lidar in flat and engineered landscapes. *Water Resources Research*, *48*(W03528). doi:10.1029/2011WR010958.

Passalacqua, P., J. Hillier, & P. Tarolli. (2014). Innovative analysis and use of high-resolution DTMs for quantitative interrogation of earth surface processes. *Earth Surface Processes and Landforms*, *39*, 1400-1403. doi: 10.1002/esp.3616.

Pelletier, J.D. (2013). A robust, two-parameter method for the extraction of drainage networks from high-resolution digital elevation models (DEMs): Evaluation using synthetic and real-world DEMs. *Water Resources Research*, *49*, 1-15. doi: 10.1029/2012WR012452.

Perron, J.T., J.W. Kirchner, & W. E. Dietrich. (2008). Spectral signatures of characteristic spatial scales and nonfractal structure in landscapes. *J. Geophys. Res., 113*(F04003). doi:10.1029/2007JF000866.

Roering, J.J., B. Mackey, J. Marshall, K. Sweeney, N. Deligne , A. Booth, A. Handwerger, & C. Cerovski-Darriau. (2013). 'You are HERE': Connecting the dots with airborne lidar for geomorphic fieldwork. *Geomorphology*, *200*, 172-183. doi: 10.1016/j.geomorph.2013.04.009.

Sangireddy, H., C. Stark, A. Kladzyk, & P. Passalacqua. (in review). GeoNet: An open source software for the automatic and objective extraction of channel heads, channel network, and channel morphology from high resolution topography data. *Environmental Modelling & Software*.

Sofia, G., P. Tarolli, F. Cazorzi, & G. Dalla Fontana. (2011). An objective approach for feature extraction: distribution analysis and statistical descriptors for scale choice and channel network identification. *Hydrol. Earth Syst. Sci., 15*, 1387–1402.

Tarboton, D.G., R.L. Bras, & I. Rodriguez-Itrube. (1991). On the extraction of channel networks from digital elevation data. *Hydrological Processes*, *5*, 81-100.

Tarboton, D.G., R.L. Bras, & I. Rodriguez-Itrube. (1992). A physical basis for drainage density. *Geomorphology*, *5*, 59-76.

Tarolli, P., J.R. Arrowsmith, & E.R. Vivoni. (2009). Understanding earth surface processes from remotely sensed digital terrain models. *Geomorphology*, *113*, 1–3. doi:10.1016/j.geomorph.2009.07.005.

Tarolli, P., G. Sofia, & G. Dalla Fontana. (2012). Geomorphic features extraction from high-resolution topography: landslide crowns and bank erosion. *Natural Hazards*, *61*, 65–83. doi: 10.1007/s11069-010-9695-2.

N. Wiener. Extrapolation, interpolation, and smoothing of stationary time series, with engineering applications. [Cambridge]: Technology Press of the Massachusetts Institute of Technology, 1949.

Youn, C., V. Nandigam, M. Phan, D. Tarboton, N. Wilkins-Diehr, C. Baru, C. Crosby, A. Padmanabhan & S. Wang. (2014). Leveraging XSEDE HPC resources to address computational challenges with high-resolution topography data. Proceedings of the 2014 Annual Conference on Extreme Science and Engineering Discovery Environment, Atlanta, GA, USA, July 13-18, ACM. doi: 10.1145/2616498.2616564.